Feb-24-2020

Cycling Phosphorus on the Archean Earth: Part II. Phosphorus Limitation on Primary Production in Archean Ecosystems

Authors: Jihua Hao[1,2*], Andrew H. Knoll[3], Fang Huang[4,5], Juergen Schieber[6], Robert M. Hazen[7], Isabelle Daniel[1]

*Corresponding author: haojihua@gmail.com

[1]Univ Lyon, Université Lyon 1, Ens de Lyon, CNRS, UMR 5276 LGL-TPE, F-69622, Villeurbanne, France

[2]Department of Marine and Coastal Sciences, Rutgers University, New Brunswick NJ, 08901, USA

[3]Department of Organismic and Evolutionary Biology, Harvard University, Cambridge MA 02138, USA

[4]Tetherless World Constellation, Rensselaer Polytechnic Institute, Troy NY, 12180, USA

[5]CSIRO Mineral Resources, Kensington, WA 6151, Australia

[6]Department of Earth and Atmospheric Sciences, Indiana University, Bloomington, IN, 47405, USA

[7]Geophysical Laboratory, Carnegie Institution for Science, Washington DC, 20015, USA

Abstract:

Several lines of evidence point to low rates of net primary production (NPP) in Archean oceans. However, whether Archean NPP was limited by electron donors or nutrients, particularly phosphorus (P), and how these factors might have changed over a billion years of recorded Archean history, remains contentious. One major challenge is to understand quantitatively the biogeochemical cycling of P on the early Earth. In Part I of this series (Hao et al., 2020), we estimated the weathering flux of P to the oceans as a function of temporally increasing continental emergence and elevation through Archean time. In Part II, we conduct thermodynamic and kinetic simulations to understand key processes of P cycling within the Archean ocean, including seafloor weathering, recycling of organic P, the solubility and precipitation of secondary phosphate minerals, and the burial diagenesis of P precipitates. Our calculations suggest low solubilities of apatite minerals in Archean seawater, primarily due to nearly neutral pH and high levels of Ca. This low solubility, in turn, implies a negligible contribution of apatite dissolution to P bioavailability in Archean seawater.

We also simulate the solubility limits of common secondary P-bearing minerals, showing that vivianite would have been the least soluble P mineral in ferruginous Archean seawater (0.1 to 0.3 μM), even at moderate supersaturation states (Ω = 100 or 1000). If vivianite precipitation was kinetically favorable by microbial activities and mineral adsorption, the sinking flux of P as vivianite in Archean seawater could have reached the modern sinking flux, implying that vivianite precipitation was a potentially major sink for P in Archean oceans. During burial diagenesis, however, vivianite in porewater would have become less stable than Ca-phosphates of lower solubility. At elevated temperatures (>100 °C) associated with burial diagenesis and low-grade metamorphism, vivianite is predicted to react irreversibly with calcite to form apatite.

Optimistic assumptions about the recycling efficiency of P on the Archean Earth lead us to estimate that by the end of the eon the total flux of P (continental weathering + recycling) could have supported NPP at levels up to 7 % of the modern. The total flux of P would have been much lower on the early and middle Archean Earth, whereas fluxes of electron donors could have been higher, suggesting very low productivity and P-limitation of marine ecosystems during much of the eon. Comparing our estimates of NPP as limited by P supply with the estimate by Ward et al. (2019), in which NPP was limited by electron donors and metabolic efficiency, there could have been a transition between P-limited productivity in the early to middle Archean to electron donor-limitation closer to the eon's end (assuming no oxygenic photosynthesis). Once oxygenic photosynthesis reached ecological significance, probably near the end of the Archean, our estimated flux of P would allow rapid oxidation of atmosphere.

(466/500 words)

Keywords: vivianite; phosphorus recycling; burial diagenesis; apatite nodules; primary production; oxygenation of atmosphere. (6/6 keywords)

1. Introduction

How productive were Archean oceans? All recent estimates of Archean primary production are low (Bjerrum & Canfield, 2002; Canfield et al., 2006; Kharecha et al., 2005; Laakso & Schrag, 2018; Ward et al., 2019), but there is no consensus just how low they were, nor on the principal factors that limited photosynthesis in early ecosystems. Some commentators posit that prior to the evolution of oxygenic (cyanobacterial) photosynthesis, the global availability of electron donors would have constrained rates of primary production to low levels. For example, Canfield et al. (2006) estimated the abundances of non-water electron donors in Archean oceans, concluding that the most abundant species, Fe^{2+}, would have supported primary production at levels up to 10% of the modern. In contrast, Ward et al. (2019) argued that H_2 and, to a lesser extent, Fe^{2+} together fueled early photoautotrophy at rates well below one percent of modern levels. And recently, Tosca et al. (2019) concluded that photoautotrophy of ferrous iron could have made only a negligible contribution to productivity in early oceans. In contrast, some analyses point to nutrient limitation in early oceans, specifically suggesting that relatively low phosphate availability could have limited primary production, even at low ferrous iron availability (Kipp and Stüeken, 2017); others propose that P was relatively bioavailable, especially as phosphite (Herschy et al., 2018).

Of particular interest is the role that oxygenic photoautotrophs may have played prior to the Great Oxygenation Event (GOE) ca. 2.4 billion years ago. It has been proposed that the GOE simply reflects the evolution of oxygenic photosynthesis (e.g., Fischer et al., 2016; Kopp et al., 2005), but this view is challenged by both an increasing inventory of geochemical evidence for earlier "whiffs of oxygen" (Anbar et al., 2007; Kaufman et al., 2007) and molecular clocks that call for the evolution of coupled photosystems capable of extracting electrons from water as early as 3.2 Ga (Cardona et al., 2019). Of course, if P availability strictly limited rates of primary production on the Archean Earth, oxygen production may well

have been too low to titrate available reductants, even if oxygenic photosynthesis was relatively prominent.

To explore these issues further, we employ kinetic and thermodynamic modeling to estimate P availability in the global scale of seawater through a billion years of recorded Archean history.

2. Methods

The bioavailability of P in the sunlit ocean primarily reflects two fluxes: continental weathering and P recycling within the ocean. Considering that Archean seawater was weakly acidic (Halevy and Bachan, 2017; Krissansen-Totton et al., 2018) and reducing, seafloor weathering might also have been a significant source of P on the early Earth. In Part I of this series (Hao et al., 2020), we simulated the input of P to the Archean oceans from continental weathering and erosion, concluding that P fluxes from land were extremely low as the Archean Eon began but increased to values similar to the modern by the time the eon ended. In this study, we calculate the solubility limits of primary and secondary P-minerals in Archean seawater and porewater environments, simulating seafloor weathering and the precipitation of phosphate minerals in and beneath the Archean ocean. We focus in particular on the precipitation of vivianite, as this precipitation has been argued to be a major sink for phosphate in ferruginous Proterozoic oceans (Derry, 2015). With these calculations in hand, we assess P recycling in Archean oceans and estimate the total flux of P for net primary production (NPP). Lastly, we consider the fate of P-precipitates during diagenesis and metamorphism, based on both simulations and geological observation.

Our calculations focus on the global-scale evolution of Archean environments. We understand that the Archean Earth was environmentally heterogeneous, with probable local variations in temperature, Fe(II) concentration between seawater and hydrothermal fluids,

redox variation between globally anoxic and locally oxygenated habitats in the late Archean, and variations in the concentration of Fe(II) and S(II) between globally ferruginous seawater and regionally sulfidic seafloor in late Archean oceans. Such heterogeneities are important in considerations of Archean evolution and may influence Archean P cycling, as discussed below. Nonetheless, we argue that our focus on global conditions is most relevant for understanding the P cycle and how it changed through Archean time.

2.1 Archean seawater and porewater chemistry

The emergence of land masses in the middle to late Archean Eon (Hawkesworth et al., 2017), with its consequences for weathering and erosional fluxes, strongly affected marine geochemistry (Bindeman et al., 2018). The evolution of seawater pH and major salts (Ca and Mg) has recently been modeled independently by Halevy and Bachan (2017) and Krissansen-Totton et al. (2018), with similar results. In Part I of this series (Hao et al., 2020), we modified Krissansen-Totton et al.'s (2018) geologic carbon cycle (GCC) model by incorporating continental emergence (Flament et al., 2013; Korenaga et al., 2017) and the weathering kinetics of P, using this modification to simulate the continental flux of P into the oceans (**Table 1**). The GCC model also outputs major component compositions of the atmosphere (including $pCO_{2,g}$) and seawater (including pH, Ca^{2+}, and CO_3^{2-}), and by linking these factors to continental emergence models and solubilities of P-bearing minerals (**Table S2**) we can examine seafloor weathering and the precipitation of P in the Archean oceans (*Sec. 2.2*). In addition, the GCC model allows us to consider the chemistry of porewater, enabling us to explore the post-depositional fate of seafloor P-precipitates (*Sec. 2.5*).

In addition to the above-mentioned species, our simulations require that we input abundance values for other components of seawater and porewaters. A large, recently compiled dataset of fluid inclusions in Archean quartz from different localities supports the view that the

concentration of NaCl in Archean seawater was similar to that of the modern (Marty et al., 2018). Accordingly, we assumed that the Cl^- concentration of Archean seawater was the same as today's. F^- concentration is set to be limited by the solubility of fluorite in Archean seawater and porewater, as it is for modern seawater.

It has been proposed that Fe^{2+} in Archean seawater was limited by the solubility of amorphous greenalite, experimentally shown to precipitate readily in equilibrium with Fe(II) and silica in anoxic water (Tosca et al., 2016; Tosca et al., 2019). Consistent with these factors, greenalite occurs abundantly in marine sediments, especially in Archean sedimentary successions (Isson and Planavsky, 2018; Johnson et al., 2018). In comparison to greenalite, siderite precipitation is kinetically sluggish under Archean conditions, occurring only when $pCO_{2,g}$ reaches extreme levels, e.g. > 1 bar (Jiang and Tosca, 2019). In the absence of a skeletal silica sink, dissolved silica concentration would presumably have been relatively high, limited by the solubility of amorphous silica (Siever, 1992; Tréguer and De La Rocha, 2012). Previous workers have also pointed to green rust as a potentially major precipitate from early seawater (Halevy et al., 2017; Tosca et al., 2019), but its precipitation requires either a flux of $O_{2,g}$ or water pH > 8.0 under anoxic conditions, unlike the anoxic and weakly acidic seawater likely during most of the Archean Eon. Moreover, the precipitation of green rust is sensitive to salinity, and the potential effects of elevated Archean $SiO_{2,aq}$ on green rust precipitation remain unknown (Tosca et al., 2019). Given these considerations, we calculated the Fe^{2+} concentration in Archean seawater based on the equilibrium constant for amorphous greenalite dissolution derived from recent experiments (Tosca et al., 2016) and the assumption that $SiO_{2,aq}$ concentration was equal to the solubility of amorphous silica. Note, however, that siderite could and did form readily by biological reduction of Fe(III) or diagenesis/metamorphism of organic-C in the sediments (Vuillemin et al., 2019), and so would potentially have been an important mineral product in porewaters beneath Archean oceans (*Sec. 4.3*).

166

167 *2.2 Thermodynamic models of P-minerals solubilities*

168 We calculated the solubility limits of common primary and secondary phosphate
169 minerals based on equilibrium constants between each mineral and its dominant aqueous
170 species at a given pH in water, e.g. HPO_4^{2-} (pH > 7.2) and $H_2PO_4^-$ (pH < 7.2) as the dominant
171 phosphate species in this study (**Table S1 & S2)**. Calculations were conducted assuming a
172 warm climate (seawater temperature 25°C), supported by recent climate reconstructions
173 (Krissansen-Totton et al., 2018). Small fluctuation of temperature would be expected to result
174 in only limited changes for reaction constants (e.g. Al-Borno & Tomson, 1994). However,
175 large elevation of temperature would significantly affect reaction constants; therefore, for the
176 calculations in diagenetic and metamorphic environments, we varied temperature to investigate
177 the effect of this variable (see below). Equilibrium constants of the dissolution reactions were
178 calculated by SUPCRT92b (Johnson et al., 1992) (**Table S2)**.

179 In the modern ocean, the sinking of P is, in general, composed of (co-)precipitation of
180 authigenic minerals (**Table S1**), burial as organic-P, or adsorption onto metal-hydroxides and
181 carbonate (Baturin, 2003; Ruttenberg et al., 2014). In iron-rich, low-salinity estuaries along the
182 Baltic Sea, vivianite ($Fe_3(PO_4)_2*8H_2O$) precipitation accounts for as much as 40% of P removal
183 from ambient waters (Lenstra et al., 2018), and Derry (2015) has proposed that this mineral
184 formed an important sink for P in the ferruginous, low-sulfate seawater of mid-Proterozoic
185 oceans. Derry's hypothesis may apply, as well, to the Archean, but this possibility needs to be
186 tested for the distinct and evolving conditions of Archean seawater (pH, Fe, S, and silica). The
187 solubility constant of vivianite is adopted from a previous experimental study (Al-Borno and
188 Tomson, 1994).

189 $$Fe_3(PO_4)_2 \cdot 8H_2O_{,s} \rightarrow 3Fe^{2+} + 2PO_4^{3-} + 8H_2O \quad (1)$$

At pH < 7, $PO_4^{3-} + 2H^+ \rightarrow H_2PO_4^-$. As mentioned above, seawater Fe(II) is presumably controlled by the solubility of amorphous greenalite:

$$Fe_3Si_2O_5(OH)_{4,am} + 6H^+ \rightarrow 3Fe^{2+} + 2SiO_{2,aq} + 5H_2O \quad (2)$$

where, $SiO_{2,aq}$ is set by the solubility of amorphous silica:

$$SiO_{2,am} \rightarrow SiO_{2,aq} \quad (3)$$

We can obtain the equilibrium constant of the following reaction by combining the reaction constants of reactions (1-3):

$$Fe_3(PO_4)_2 \cdot 8H_2O_{,s} + 2SiO_{2,am} \rightarrow Fe_3Si_2O_5(OH)_{4,am} + 2H_2PO_4^- + 2H^+ + 3H_2O \quad (4)$$

In similar fashion, we compiled the reported equilibrium constants of the dissolution reactions of other common secondary P-minerals and calculated their solubility limits in the Archean seawater and porewater (**Table S2**).

2.3 Crystallization and precipitation kinetics of vivianite

We employed the crystal growth kinetics of vivianite reported previously (Madsen & Hansen, 2014; Madsen, 2019). Vivianite crystals have shown to follow spiral growth mechanism at low supersaturation states (Madsen & Hansen, 2014) with the rate expression:

$$Rs = b(c_{Fe} - c_{Fe,eq})\ln\Omega \quad (5)$$

b (nm/s/M) is rate constant, Ω is the saturation state of vivianite defined by the ratio of quotient (Q) and equilibrium constant (K) of the precipitation reaction. Considering that the Archean seawater had high concentrations of Fe^{2+} and vivianite could reach moderate to high supersaturation states (as discussed below), we assume that $c_{Fe} - c_{Fe,eq} \cong c_{Fe}$. The value of b was found to increase with increasing concentrations of Ca^{2+}; due to the limited Ca^{2+} range considered in the literature, we used 3.19 (at 6.11 mM Ca^{2+} in Madsen, 2014) as a conservative value for Archean seawater.

Following the methods proposed by Derry (2015), we simulated the precipitation rate and deposition flux of vivianite as a function of this mineral's saturation state. Simply put, the rate law for vivianite precipitation is

$$R_p = k_{eff}\left[\left(\frac{Q}{K}\right) - 1\right]^n \quad (4)$$

R_p: precipitation rate of vivianite, mole/(m^3*s); k_{eff}: 2.6 ± 0.3 × 10^{-15} mol/(m^3*s); n: 1.3 ± 0.3. The precipitation flux of vivianite is calculated by integrating the rate over the likely depth of Archean Fe(II)-rich seawater, similar to Derry (2015).

2.4 Recycling of phosphorus in Archean seas

Considering that seafloor weathering (Sec. *3.1 & 4.1*) and extraterrestrial impacts (**Table 1**) provide only small amounts of phosphorus, we assume that the total P for Archean NPP is predominantly composed of P from continental weathering and recycling within the ocean, i.e.,

$$\text{NPP(P)} = \text{Recycling-P} + \text{Weathering-P} \quad (5)$$

Assuming $R_{recycling}$ = recycling efficiency of biological P,

$$\text{Recycling-P} = R_{recycling} * \text{NPP(P)} \quad (6)$$

Therefore,

$$\text{NPP(P)} = R_{recycling} * \text{NPP(P)} + \text{Weathering-P} \quad (7)$$

And,

$$\text{NPP(P)} = \text{Weathering-P}/(1 - R_{recycling}) \quad (8)$$

According to **Table 1**, $R_{recycling}$ = 0.998 in the modern ocean, but due to a limited supply of oxidants and possible precipitation of P as vivianite in the Archean ocean, the recycling of P would have been less efficient. As discussed in detail in *Section 4.4*, we choose $0.01 < R_{recycling} < 0.78$ in the Archean ocean and, based on that value, we calculate the maximum amount of recycled P available for Archean primary producers, as reported in **Table 1**.

239

240 *2.5 Diagenetic and metamorphic transformation of vivianite: modeling*

241 In this study, we simulated the stability and solubility of various phosphate minerals
242 and other diagenetic minerals in porewater environments (**Fig. S1-2**; 25 °C), thereby
243 mimicking the early diagenesis of P in the Archean marine sediment.

244 In addition, we simulated the reaction of vivianite + calcite (+ fluorite as a source of F^-)
245 to form apatite + siderite (+ release of water) at elevated temperatures, mimicking the fate of
246 vivianite during burial diagenesis and metamorphism. The equilibrium constants of the reaction
247 were calculated by SUPCRT92b, with thermodynamic properties of vivianite from Al-Borno
248 and Tomson (1994).

249

250 **3. Results**

251 *3.1 Limitations on seafloor weathering of apatite*

252 In continental rocks, apatite is the primary P-hosting mineral for chemical weathering,
253 and detrital P, mainly as apatite, is the predominant component of continental P input to the
254 ocean system (Compton et al., 2000; Ruttenberg et al., 2014). In oceanic crust, apatite is
255 unlikely to be a major host mineral for P due to high saturation concentrations; rather P is
256 expected to exist either as trace impurities in silicate minerals — including olivine,
257 clinopyroxene, and plagioclase — or in basaltic glass (Brunet & Chazot, 2001). However, trace
258 amounts of apatite are common in basalts and gabbros (e.g., Anderson & Greenland, 1969;
259 Coogan et al., 2001; Meurer & Natland, 2001), and apatite may precipitate locally due to the P
260 gradient near a growing crystal (Green & Watson, 1982).

261 If the concentration of dissolved P in the weathering fluid reaches the solubility limit
262 of apatite, apatite as the reactant will have no reaction affinity to dissolve further (Brantley and
263 Olsen, 2014). Salinity and pH are the two most important environmental determinants of

apatite solubility. Seawater pH is primarily buffered by the riverine transport of alkalinity, seafloor weathering of silicates, and hydrothermal fluids. Although the Archean atmosphere had high $pCO_{2,g}$, simulated pH of Archean seawater ranges from 6.5 to 7.0 (Halevy and Bachan, 2017; Krissansen-Totton et al., 2018), unlike the more acidic rainwater that drove continental weathering (Hao et al., 2017). Ca^{2+} level is another important factor in determining the solubility of P. It has been proposed that Archean seawater was more enriched in Ca^{2+} than the modern oceans because of enhanced hydrothermal alteration of the seafloor (Halevy and Bachan, 2017; Jones et al., 2015; Krissansen-Totton et al., 2018).

Based on these considerations, and applying our additional assumptions for Archean seawater composition (**Methods**), we calculated the solubility limits for three common types of apatite: Cl-apatite, F-apatite, and OH-apatite. **Fig. 1** shows that all three minerals had limited solubility (< 0.1 μM; predominantly as $H_2PO_4^-$ at pH < 7) in Archean seawater; results are consistent whether one assumes rapid or slow continental emergence on the late Archean Earth. The low solubility of apatite minerals in Archean seawater contrasts markedly with their high solubilities in contemporaneous continental weathering fluids (Hao et al., 2017), a difference primarily ascribed to the higher pH and higher concentrations of Ca^{2+} and halogens in Archean seawater, relative to rain or river water (Hao et al., 2020). In addition, the log dissolution rate of apatite minerals decreases linearly with increasing pH in acidic water (Brantley and Olsen, 2014; Guidry and Mackenzie, 2003). Thus, in Archean oceans, the weathering of apatite was both thermodynamically and kinetically less favorable than continental weathering. Indeed, the direct implication of **Fig. 1** is that seafloor weathering of apatite minerals could have contributed little if any P to early marine life. Consistent with these simulation results, we observed detrital apatite as the major P-phase in Archean black shales, with tiny overgrowths of secondary apatite (Bothaville Formation, South Africa; ca. 2700 Ma) (Fig. 7a & b). Bothaville sediments reflect rapid uplift and erosion of a crustal bloc to the west (Schneiderhan

et al., 2011), resulting in large input of P with a major proportion being detrital apatite minerals (Hao et al., 2020). In addition, as discussed in *Sec. 4.1*, we think that seafloor weathering of basalt would contribute little P to early oceans.

3.2 Solubility and precipitation of secondary phosphates in the Archean seawater

On the modern Earth, seafloor weathering serves as a net sink for P that balances continental input (Compton et al., 2010), with P removal occurring mainly as organic-P, various authigenic/biogenic phosphate minerals (CFA, HAP, and other phosphates), and surface adsorption onto or co-precipitation with Fe(III)-(hydr)oxide and carbonate (Ruttenberg et al., 2014). In anoxic Archean seawater, Fe(II) oxidation could and did occur via photo- and/or bio-oxidation of Fe(II), or the cooling of hydrothermal fluids, as documented by ferric iron in Archean banded iron formations. Several investigators analyzed the P content in BIFs in order to reconstruct paleo-concentrations of P, assuming that adsorption onto Fe-(hydr)oxide was the major sink for P (Jones et al., 2015; Konhauser et al., 2007; Planavsky et al., 2010).

In addition to surface adsorption, however, our simulations suggest that vivianite would have a much lower solubility in Archean seawater than other secondary P-minerals (e.g. octacalcium phosphate, or OCP) (**Table S1** and **Fig. 2**). Assuming a moderate supersaturation state of vivianite, Ω = 100 or 1000, our calculations indicate that phosphate solubility in Archean oceans would have been similar to that estimated by Jones et al. (2015), 0.1 to 0.3 μM dissolved phosphate depending on Ω and age (**Fig. 2**). This estimate depends heavily on the feasibility of vivianite precipitation, experimentally shown to be sluggish at low supersaturation but potentially facilitated by microbial reduction and mineral adsorption in natural systems (Sec. *4.2*). Regardless, in the low-P Archean seawater, octacalcium phosphate (OCP) as the precursor phase of marine apatite (Van Cappellen, 1991) has no thermodynamic affinity to precipitate. Undersaturation of OCP in the Archean seawater further indicates that,

314 precipitation of apatite minerals, although thermodynamically favorable given their extremely
315 low solubilities (**Fig. 1**), was not kinetically feasible (Gunnars et al., 2004).

316 Using the reported crystallization kinetics of vivianite (Madsen & Hansen, 2014;
317 Madsen, 2019) and assuming the presence of mineral seed, we estimated 46-695 μm crystal
318 growth for 1 year at supersaturation states of 100-1000 in the Archean seawater (**Fig. 3a**;
319 assuming 0.1 to 1 mM Fe^{2+}), this falling into the size range of vivianite nodules found in natural
320 sediments at low supersaturation states (Rothe et al., 2016). Following the method proposed
321 by Derry (2015), we calculated the precipitation rate of vivianite from water column to
322 sediment, showing that the depositional flux of P as vivianite in the Archean oceans could
323 easily have reached levels comparable to the modern sinking flux for P at $\Omega > 10$ (i.e., solubility
324 of P = 0.03 μM) (**Fig. 3b**). Derry's model assumes ready vivianite precipitation even at low
325 supersaturation states, but the actual precipitation flux should depend heavily on precipitation
326 kinetics of vivianite, which is known to be affected by a number of factors (Sec. *4.2*).

327

328 *3.3 Post-depositional transformation of vivianite*

329 As discussed above, vivianite precipitation could be an important P sink in Archean
330 oceans. The fate of vivianite during diagenesis and metamorphism, however, requires
331 consideration.

332 Assuming that siderite and greenalite precipitation could reach in equilibrium, our
333 simulations show that in the porewater environment siderite solubility is 2 to 4 orders of
334 magnitude lower than greenalite (**Fig. 4a & S3a**). Therefore, if siderite precipitation becomes
335 kinetically feasible during burial diagenesis (Sec. *4.3*), it should limit the solubility of Fe(II) to
336 low values, as argued for Archean porewaters (Tosca et al., 2019). Under these conditions,
337 vivianite becomes much more soluble than other secondary phosphate minerals, e.g.
338 octacalcium phosphate (OCP) and carbonate fluorapatite (francolite) (**Fig. 4b & S3b**). OCP is

thought to be the precursor phase of marine apatite minerals (Eanes & Meyer, 1977; Van Cappellen, 1991). In the modern marine sediments, precipitation of P as apatite minerals is thought to one major P sink in the long run (Ruttenberg, 2014; Van Cappellen, 1991). Our simulations show that in the Archean porewaters, the solubilities of apatite minerals are expected to be extremely low (at least 1-3 orders of magnitude lower than OCP and 5-9 orders of magnitude lower than vivianite; **Fig. 4c**), implying strong thermodynamic affinity for the transformation from vivianite to OCP and apatite minerals (*Sec 4.3*).

In addition, we calculated the reaction constant for the transformation of vivianite + calcite (+ fluorite; with a fluorine level similar to the seawater) to F-apatite + siderite (with release of water) at elevated temperatures, mimicking the burial diagenesis and low-grade metamorphism of vivianite. The result suggests that log (reaction constant) is >> 1, and its value increases with temperature (**Fig. 5**), suggesting that the transformation becomes thermodynamically more and more favorable. Therefore, it can be reasonably expected that at the elevated temperatures of burial diagenesis and metamorphism (> 100 °C, where the precipitation kinetics of apatite and siderite are feasible), vivianite would inevitably transform to apatite.

3.3 Total phosphorus for Archean primary production

Fig. 6 shows the proportional contribution of continental weathering to the total P requirement for NPP as a function of recycling efficiency. In line with the hypothesis by Laakso & Schrag (2018), the figure indicates that on the Archean Earth, continental weathering would provide the major source of P for life in photic zone, unlike today. Based on our estimate of continental P flux (**Table 1**) and a recycling efficiency of 0.78 (Sec. *4.4*), we calculate the recycling flux of organic P by the end of the Archean Eon to have been 14-120 $\times 10_{10}$ moles P/yr (**Table 1**). Note that the flux of recycling P, which represents an optimistic estimate in this

study, depends heavily on the recycling efficiency (and thus burial efficiency) of organic matter in the Archean Eon, which is poorly constrained (Kipp et al., 2019) and might have evolved through time (Sec. *4.4*). Assuming deep water P concentrations equivalent to 10% of the modern value and a typical vertical mixing rate (3 m/yr), Ward et al. (2019) recently estimated Archean P recycling to have been $40 \times 10_{10}$ moles P/yr, within the range of our values. Regardless of uncertainties, these estimates agree that the recycling flux of P in late Archean oceans was 1-2 orders of magnitude lower than today's (about $3710 \times 10_{10}$ moles P/yr; Schlesinger and Bernhardt, 2013). Together with our estimated continental input of P, up to $18\text{-}154 \times 10_{10}$ moles P/yr would have been available for marine primary productivity by the end of Archean Eon, 0.5-4% of modern values (**Table 1**). Because of limited continental emergence and elevation, the continental flux of P and thus the recycling flux of P would have been much smaller on the earlier Archean Earth, perhaps $< 0.05 \times 10_{10}$ moles P/yr, i.e. 0.001 % of the modern value (**Table 1**).

4. Discussion

4.1 Seafloor weathering of phosphorus

In the modern ocean, seafloor weathering is widely agreed to be a net sink for P, primarily due to surface adsorption onto Fe(III)-hydroxide or carbonate (Wheat et al., 1996) or (co)precipitation of P-minerals (hydroxylapatite, CAP, REE/Al-phosphates) (Ruttenberg et al., 2014). Given the reducing and weakly acidic nature of Archean seawater, however, dissolution of basaltic glass has been proposed as a source of P for autotrophs (Kakegawa, 2003). To date, there is limited evidence to support this hypothesis. Syverson et al. (2020) recently observed slight P release during alteration of basalt at 25 °C under anoxic conditions, whereas alteration experiments under oxic condition did not show any P release. These observations seemingly support seafloor weathering as a potential source of P in the anoxic Archean ocean(s). However,

389 Syverson et al. used a simulated seawater solution without any inorganic C, which diverges
390 markedly from realistic estimates of Archean seawater chemistry (high $CO_{2,aq}$ and
391 (bi)carbonate species; Halevy & Bachan, 2017; Krissansen-Totton et al., 2018). Under these
392 more realistic conditions, seafloor weathering would precipitate abundant carbonate minerals,
393 a major sink in the Archean carbon cycle (Krissansen-Totton et al., 2018) as well as a known
394 mineral product in modern seafloor weathering. Carbonate minerals have a strong affinity to
395 phosphate and could limit soluble P by either surface adsorption (de Kanel & Morse, 1978;
396 Millero et al., 2001; Wheat et al., 1996) or co-precipitation as carbonate apatite (Freeman &
397 Rowell, 1981; Rubinstein et al., 2012; Xu et al., 2014); both represent a major sink for P in
398 modern carbonate-rich and/or anoxic sediments (e.g. Baturin, 2003; Fourqurean et al., 1992;
399 Kraal et al., 2017). In addition, elevated temperature or presence of divalent cations (e.g. Ca^{2+},
400 Mg^{2+}) would increase uptake of phosphate by carbonate (Millero et al., 2001). In fact,
401 carbonate minerals can capture $2.3 – 4.5 * 10^{12}$ mole P/yr in the modern ocean, 2 - 4 times the
402 sink provided by hydrothermal iron hydroxides (Baturin, 2003); carbonates could be expected
403 to form a larger sink in the Archean due to higher $pCO_{2,g}$ and highly weatherable rocks.
404 In another study, Murakami et al. (2019) investigated the hydrothermal alteration of
405 basalt under CO_2-rich condition (+ 30 mmole/kg Ca^{2+}), mimicking Archean atmospheric and
406 seawater composition. Their experiments revealed under high CO_2 conditions, carbonate was
407 a major alteration product, with higher P-uptake than occurred in a CO_2-free run, supporting
408 the hypothesis that carbonate minerals would take up phosphate released from seafloor
409 weathering or via diffusion from seawater. A limited contribution of P from glass weathering
410 is further supported by the observations of modern and Archean glasses altered under anoxic
411 conditions; these showed enrichment or no loss of P (Alt & Honnorez, 1984; Rubinstein et al.,
412 2012; Staudigel et al., 2008). In addition to uptake by carbonates, there are other substantial
413 sinks of P during seafloor weathering, including the precipitation of Al/REE phosphates (Byrne

& Kim, 1993; Rasmussen, 2000) and vivianite (this study; Derry et al., 2015). Based on the above considerations, we argue that seafloor weathering should be a negligible source and possibly a large sink in the Archean P cycle.

4.2 Vivianite precipitation kinetics

Direct precipitation of vivianite from Fe(II)-PO_4 solution has been experimentally shown to be kinetically inhibited at low saturation states under ambient conditions (Walpersdorf et al., 2013). In addition, at low supersaturation states, vivianite precipitation has been shown to follow spiral growth mechanism, at rates slower than surface-nucleation growth at high supersaturation states (Madsen & Hansen, 2014; Madsen, 2019). Altogether, slow kinetics of precipitation and crystallization might indicate a relatively minor role for vivianite as a P sink in Archean oceans. Indeed, Johnson et al. (2020) suggested that vivianite was not a major P sink in the ferruginous sediments of the Mesoproterozoic Sherwin Ironstone despite the high supersaturation states predicted by thermodynamic models. However, in modern Fe(II)-rich anoxic waters (Cosmidis et al., 2014) and sediments (Borch & Fendorf, 2008; Jilbert & Slomp, 2013; Sánchez-Román et al. 2015), vivianite precipitation can be facilitated by microbial reduction of Fe(III) in presence of phosphate. In addition, phosphate adsorbed into ferrous minerals, e.g. green rust, has been shown to quickly transform into vivianite (Hansen & Poulsen, 1999; Xiong et al., 2019). The presence of mineral seeds (e.g. quartz) could also facilitate the crystallization of vivianite and lower the supersaturation demand (Liu et al., 2018). These mechanisms may explain the precipitation of vivianite at low to moderate supersaturation states in modern anoxic waters ($\Omega = 40$ for lake Pavin; Cosmidis et al., 2014) and sediments ($\Omega < 1$ for Baltic Sea porewater; Jilbert & Slomp, 2013; $\Omega < 1000$ for Lake Groß-Glienicke and Lake Arendsee porewaters, although Lake Spitzingsee porewater vivianite is absent at $\Omega > 10000$; Rothe et al., 2016), which might also have been true for Archean oceans.

Given these uncertainties, we cannot provide a quantitative estimate for the sedimentation flux of phosphate as vivianite in Archean oceans and thus evaluate the importance of vivianite precipitation as a P sink. Global vivianite fluxes would be greatly affected by poorly constrained concentrations and fluxes of phosphate and ferrous iron in Archean seawater. Moreover, the precipitation kinetics of vivianite are strongly influenced by temperature (Madsen & Hansen, 2014), microbial activity (Borch & Fendorf, 2008), and mineral surface (Hansen & Poulsen, 1999; Liu et al., 2018; Xiong et al., 2019). Additionally, adsorption onto Fe-(hydr)oxide (Bjerrum and Canfield, 2002; Jones et al., 2015) or green rust (Zegeye et al., 2012) and/or co-precipitation as Fe(III)-phosphate would have competed for P with vivianite precipitation in surface seawater, and these processes cannot be quantified on the basis of available information. Nevertheless, we support the qualitative argument that the global flux of P precipitated by vivianite was important in the Archean P cycle, limited largely by the input of P from continental weathering and riverine transport (**Table 1**).

4.3 Burial of P in the Archean marine sediments

Within sediments, precipitation of siderite could become kinetically feasible during diagenesis through bioreduction of Fe(III) in the presence of organic matter (Vuillemin et al., 2019) or via burial heating. Our simulations suggest that siderite precipitation would minimize the solubility of Fe(II) (**Fig. 4a**); as a result, sedimentary vivianite would have higher solubility than calcium phosphates (**Fig. 4b & 4c**). Under these circumstances, vivianite becomes unstable with respect to calcium phosphates, and the dissolution of vivianite could result in higher P than OCP and francolite solubility in porewater (Thinnappan et al., 2008), inducing OCP or francolite precipitation. OCP has been suggested as essential precursor phase for apatite precipitation (Gunnars et al., 2004; Van Cappellen, 1991) and the presence of OCP could facilitate the precipitation of apatite, which would continue until P levels declined to

values lower than OCP solubility (Nancollas, 1984; Van Cappellen, 1991). Given the much lower solubility of apatite minerals than vivianite and OCP (**Fig. 4c**), precipitation of apatite should be a significant P-sink, maintaining low levels of P in Archean porewater (< 1 μM as the solubility of OCP in **Fig. 4b**).

Other forms of deposited P, including Fe(III)/Al-hydroxide or carbonate bound- and organic-P, might also transform into calcium phosphates, along with the reduction of Fe(III) and breakdown of organic matter in porewater environments. Indeed, transformation of Al/Fe(III)-bound P to OCP has been observed in modern nearshore sediments and shown to be facilitated by increasing pH and/or decreasing Eh (Oxmann & Schwendenmann, 2015). In modern anoxic sediment, it has been observed that organic-P could transform progressively into calcium phosphate with the aid of $CaCO_3$ during burial diagenesis (Kraal et al., 2017). Archean porewaters were probably enriched in Ca (**Fig. S1-2**) and enhanced seafloor weathering at high $pCO_{2,g}$ would induce widespread precipitation of $CaCO_3$ in sediments (Sleep & Zahnle, 2001). Thus, as argued for vivianite, organic-P would also transform into calcium phosphates during burial diagenesis, depending on the relative concentrations of Ca^{2+} and Fe^{2+} and ambient pH in sediments. Recently, Johnson et al. (2020) reported carbonate fluorapatite as the major phosphate in a Mesoproterozoic ferruginous sediment, probably transformed from Fe(III)-bound or organic P during burial diagenesis, supporting the hypothesis that precipitation of calcium phosphates as the dominant long-term P-sink.

We also note that the present day mineralogy of iron formations is thought to bear the strong imprint of diagenesis, including supergene enrichment (Rasmussen et al., 2016). Therefore, the current Fe and P mineralogy of Archean BIFs may not provide a strong test of our or any other low-temperature environmental hypotheses. Ca-rich carbonate would be a major product of seafloor weathering under a high $pCO_{2,g}$ Archean atmosphere (Sleep and Zahnle, 2001), its solubility increasing with rising burial pressure. $CaCO_3$ dissolution has been

shown to aid long-term sequestration of P in the sediments of modern anoxic basins by facilitating the precipitation of Ca-P minerals (Kraal et al., 2017; Krajewski et al., 1994). Therefore, in the long term, progressive burial might have converted vivianite to less soluble apatite.

Consistent with these considerations, tiny spheroids of apatite (**Fig. 7**) have been observed in Archean and Proterozoic carbonaceous shales (several % TOC) from multiple and widely separated localities. These spheroids typically measure 2 to 5 micrometers in diameter and may form solid spheres as well as thick- or thin-walled shells (**Fig. 7**). The illustrated Archean example (Bothaville Formation, South Africa; ca. 2700 Ma) shows predominantly detrital grains with small later diagenetic overgrowths (**Fig. 7a-b**). In essence, this coexistence suggests that apatite was originally deposited as a detrital component from continental erosion; in places where P concentrations reached saturation for apatite overgrowth, diagenetic overgrowths started to fill in adjacent pore space. In contrast to the Archean samples, common to all of the Proterozoic precipitates are micron-sized spheres or shells that consist of radiating apatite crystals that in places may extend beyond the apparent original sphere or shell margin outline (**Fig. 7c-f**). Thin-walled shells commonly show variable degrees of deformation, suggesting that apatite nucleated on partially degraded cell walls or extracellular envelopes. In places, multiple spheres are joined together to form a single mineralized entity (Schieber et al., 2007). The clustering of spheroids (**Fig. 7c, d, e**), the apparent progression from mineralized membranes, to thick-walled shells and solid spheres (**Fig. 7f**), and the commonly observed association with organic matter are suggestive of an organic origin, possibly as mineralized microbes that were associated with decaying organic matter (Schieber et al., 2007).

The microspheres are consistent with P liberation during organic remineralization, followed by vivianite/OCP precipitation and, later, eventually transformation to apatite during diagenesis, although we cannot reject the alternate possibility that phosphorus precipitated

originally as apatite. In either case, however, P liberated by organic remineralization did not return to the water column, but rather was immobilized by mineral precipitation.

In recent experiments, Herschy et al. (2018) documented the partial reduction of orthophosphate (PO_4^{3-}) into phosphite (PO_3^{3-}) by Fe(II) at 180 °C, mimicking burial diagenesis. This mechanism is possible, but it has little influence on our conclusions, as even under favorable conditions only about 5% of precipitated phosphate would be reduced to phosphite (Herschy et al., 2018). We note as well that the research in question did not include Ca (either aqueous species or carbonate) in the experimental system. Ca would significantly favor the stability of apatite $Ca_5(PO_3)_3(OH,F,Cl)$ against reduction of orthophosphate at the elevated temperatures and pressures associated with diagenesis and low-grade metamorphism (**Fig. 5**). This inference is consistent with evidence that apatite is the dominant P-mineral in ancient sedimentary rocks (Friend et al., 2008; Lepland et al., 2002).

4.4 Recycling of P in the Archean ocean

In the modern ocean, continental input of bioavailable P accounts for less than 1% of the P requirement for net primary production (NPP) (**Table 1**; Schlesinger & Bernhardt, 2013); the recycling of biological phosphate within the ocean overwhelmingly dominates P supply to the photic zone. On the Archean Earth, however, when the atmosphere and oceans were largely reducing, a lack of oxidants would have suppressed the recycling efficiency of biological P (Kipp and Stüeken, 2017). And, as already introduced, our simulation shows that precipitation of secondary phosphates as vivianite or Ca-phosphates might also maintain low concentrations of dissolved P in Archean seawater and porewater, impeding the recycling of phosphate freed via organic matter remineralization. Therefore, the recycling of biological P was very likely much weaker in Archean oceans and, accordingly, NPP must have been much lower.

538 The recycling efficiency of organic matter is inversely proportional to the burial
539 efficiency of NPP, which depends on the availability of oxygen (Hedges et al., 1999) and other
540 oxidants, as well as bioturbation (Zonneveld et al., 2010). Indeed, burial efficiency has an
541 inverse relationship with exposure of oxygen (as well as other oxidants), and extrapolation of
542 the correlation to zero oxygen exposure results in 40-50% burial efficiency (Hartnett et al.,
543 1998). Moreover, it has been estimated that burial efficiency can be as high as 22-32% in
544 modern ferruginous lakes (Crowe et al., 2011; Katsev & Crowe, 2015, Kuntz et al., 2015),
545 although transferring this estimate to the entire ocean needs further investigation. In contrast,
546 the burial efficiency of oceanic NPP is about 0.1% in modern oceans (Hedges and Keil, 1995)
547 Modern lakes certainly have greater inventories of oxidants (O_2, SO_4^{2-}, NO_3^-) than
548 Archean seawater. Input of sulfate would also undermine the burial P as vivianite by lowering the
549 solubility of Fe(II) in anoxic waters and sediments (Rothe et al., 2015); however, the Archean
550 seawater was depleted in sulfate (Lyons & Gill, 2010). Such considerations suggest that the
551 recycling efficiency of biological P would have been even lower in Archean oceans than in
552 modern ferruginous lakes, i.e. $R_{recycling} < 0.68\text{-}0.78$ in the Archean (**Fig. 6**). As noted above, an
553 independent approach by Ward et al. (2019) resulted in similar estimate for the flux of recycled
554 P toward the end of the Archean, supporting a lower recycling efficiency of P than the modern
555 value (~0.997).
556 Recently, Kipp & Stueken (2017) compiled the availability of oxidants for recycling P
557 through Earth history and used these to argue that rates of P recycling in Archean seawater
558 were 100 times lower than the modern, i.e., a recycling efficiency < 0.01. Kipp & Stueken's
559 estimate should represent a lower limit of recycling efficiency, considering the preferential
560 release of P during organic decomposition (Clark et al., 1998) and photo-oxidation of organics
561 in surface seawater (see below). Moreover the absence of zooplankton and fecal pellets in the

562 Archean ocean might have led to less efficient deposition of particulate organic carbon (Logan
563 et al., 1995) and, consequently, burial of organic matter in the Archean ocean.

564 It is also important to ask whether the recycling efficiency of nutrients might have
565 evolved through Archean time as a function of the redox state of surface environments (Hao et
566 al., 2019) and continental emergence (thus, shelf area for upwelling; see Olson et al., 2019).
567 In the early Archean, when surface environments were more reducing and emergent continents
568 were minimal, recycling of organic matter would be severely depressed due to oxidant
569 limitation and limited shelf area for upwelling. However, in the middle to late Archean, oxidant
570 inventories increased (Stueken et al., 2012) and continental lands increasingly emerged above
571 sea level (Flament et al., 2013; Korenaga et al., 2017). Back reduction of river-transported
572 sulfate might have depleted dissolved seawater Fe(II) regionally, even generating euxinic areas
573 in the late Archean ocean (Reinhard et al., 2009). The solubility of vivianite would increase
574 significantly in regionally euxinic zones, engendering a simultaneous increase of P solubility.
575 As a consequence, the recycling efficiency of nutrients would be expected to increase.

576 In modern surface seawater, dissolved organic P (DOP) can reach significant levels,
577 sometimes even higher than dissolved inorganic P (Ruttenberg. 2014). Due to the high stability
578 of biomolecules under reducing conditions, organic P might have also been important in the
579 Archean seawater. However, experimental studies have suggested that the lifetime of organic-
580 P under UV radiation would be short (Francko & Heath, 1979). Thus, high UV radiation, due
581 to the lack of an Archean ozone shield, might efficiently destroy organic P in the surface layers
582 of Archean seawater. Therefore, dissolved organic P might have played a relatively minor role
583 for the Archean life in photic zone.

584

585 *4.5 Electron vs. phosphorus limitation on Archean primary production?*

How do the simulations presented here inform the debate about nutrient versus electron donor limitation on net primary production (NPP) in Archean oceans? Total fluxes of electron donors on the Archean Earth have been proposed in several studies (Canfield et al., 2006; Kharecha et al., 2005; Ward et al., 2019), but estimated values vary markedly (**Fig. 8**). By comparison, fluxes of nutrients have been less commonly investigated (Laakso and Schrag, 2018; Ward et al., 2019), particularly for phosphorus, thought to be the most probable limiting nutrient. [It has been proposed that nitrogen limits global primary production on geologic time scales (Falkowski, 1997), but at the low levels for Archean NPP advocated here, nitrogen demand could have been met by modest rates of biological nitrogen fixation, and, especially during the early Archean, might have been sustained in most times and in many places by abiotic N-fixation (Chameides and Walker, 1981; Ward et al., 2019; Wong et al., 2017).]

Various lines of evidence support the concept of a more or less low-P Archean ocean (Bjerrum and Canfield, 2002; Jones et al., 2015; Planavsky et al., 2010; Reinhard et al., 2017). Here, we estimate that the total flux of P could have reached 18-154 $\times 10_{10}$ moles P/yr by the end of the Archean Eon. Assuming a standard Redfield C:P of 106:1, this is equivalent to a NPP of 19-163 $\times 10_{12}$ moles C/yr, or 0.5-4% of the modern value (ca. 4000 $\times 10_{12}$ moles C/yr; Field et al., 1998). In the modern ocean, Redfield ratios of individual populations vary within limits set by the fundamental biochemical composition of their constituent cells (Geider and La Roche, 2002). If, following Laakso and Schrag (2018), we accept that mean C:P could have reached values as high at 195:1, the total flux of P could have supported up to 7% of the modern NPP by the end of the Archean Eon. This level of NPP is higher than the estimate by Ward et al. (2019), i.e. < 0.1% for the late Archean time limited by the availability of electron donors and the efficiency of anoxygenic photosynthesis.

We stress, however, that our estimated P flux varies markedly through a billion years of recorded Archean history (Hao et al., 2020; **Figure 8**). Early in the Archean, when

611 continental weathering of P was severely limited by continental exposure and elevation, the
612 weathering and erosional flux of P from continents would have been extremely low (**Table 1**).
613 Because of this factor and limitations on recycling efficiency from both low oxidant supply
614 and the probability of P capture by vivianite, P supplied by recycling would also have been
615 extremely low (**Table 1**). Moreover, the limited area of emergent continents and, thus, coastal
616 continental margin shelf could result in relatively weak upwelling, and in consequence, reduced
617 nutrient recycling (Olson et al., 2019). P, then, could have limited NPP to less than 0.05×10^{12}
618 moles C/yr, a factor of eight lower than Ward et al.'s estimate for an Archean biosphere fueled
619 by anoxygenic photosynthesis and far lower than the value estimated by Canfield et al. (2006).
620 Altogether, these results might indicate transition from a P-limited biosphere in the early
621 Archean to an electron donor-limited biosphere as continents emerged toward the end of
622 Archean (**Fig. 8**).

623 Questions of NPP limitation by P or electron donors are straightforward only in a world
624 without oxygenic photosynthesis. Once bacteria evolved the capacity to split water, the supply
625 of electron donors became essentially unlimited and primary production would, forever after,
626 be limited by nutrient availability, primarily phosphorus (Tyrrell et al., 1999). Despite
627 continuing debate about when oxygenic photosynthesis first evolved, there is a consensus that
628 the oxygenation of atmosphere at 2.4 Ga required oxygenic photosynthesis. Ward et al. (2016)
629 simulated the oxygenation time of the Archean atmosphere under a series of settings (primary
630 production, burial fraction, and methanogenic fraction) and suggested that with a primary
631 production of 10^{14} moles C/yr, irreversible oxygenation of atmosphere would happen within ~
632 100 kyr. This level of primary production falls into the range of NPP supported by our
633 estimation of total P in the end of Archean Eon (**Table 1**). Therefore, increasing emergence of
634 continents and riverine transport of phosphorus would lead to higher primary productivity and

once oxygenic autotrophs attained ecological prominence, rapid oxygenation of atmosphere as the Proterozoic Eon began.

5. Conclusions

The total flux of P for marine ecosystems predominantly reflects input from continental weathering and the recycling of P within the ocean. Archean seawater was anoxic, with a limited supply of oxidants, suppressing P recycling and so linking primary production more closely to continental weathering. Although Archean seawater was weakly acidic, apatite solubility would have been very low due to high levels of Ca and halogens; for this reason, seafloor weathering of P should not have been a major source of P for Archean marine ecosystems. In addition, the solubility of vivianite is predicted to have remained very low (0.1 to 0.3 μM) at moderate supersaturation states (Q/K = 100 to 1000) in Archean ferruginous seawater. Under these conditions, the precipitation flux of vivianite could have reached a level comparable to or higher than the modern sinking flux for P; therefore, it might have been a major sink in the Archean P cycle, with precipitation kinetically facilitated by microbial metabolism and mineral adsorption. Although potentially delivered to accumulating sediments, vivianite would not have been stable during burial diagenesis and metamorphism, reacting readily with calcium carbonate to form more stably calcium phosphates, particularly apatite.

Together with continental input of P, our current estimate of recycling P in the Archean ocean would, under the most favorable circumstances, have allowed up to 7% of modern NPP by the end of the Archean Eon. However, during the early and middle Archean, inputs of continental weathering and P recycling would have been considerably weaker, and the fluxes of electron donors higher. Therefore, NPP of the Archean marine ecosystems may well have been limited by the availability of P instead of electron donors during most of the Archean Eon. Indeed, on the early Archean Earth, NPP may well have been too low to oxygenate the

atmosphere and surface ocean, even if oxygenic photoautotrophs were widely distributed in marine and fresh waters. Therefore, rapid oxygenation of the atmosphere might only have become possible as increasing P fluxes from weathering and erosion increased near the end of Archean Eon.

Acknowledgements We thank Dimitri A. Sverjensky, Cin-Ty Lee, Nicolas Coltice, Ciaran Harman, Mathew Pasek, Michael Kipp, David Catling, Lu Pan, Chao Liu, Liyan Tian, Ming Tang, Joshua Krissansen-Totton, Dustin Trail, and Paul Falkowski for helpful discussions. We also appreciate constructive comments by three anonymous reviewers, Nicolas Tosca, and Jeffrey Catalano. JHH & ID thank French National Research Agency (#ANR-15-CE31-0010), JHH & RMH thank NASA's Astrobiology Institute grant (80NSSC18M0093), and JHH, AHK, FH, and RMH thank W.M. Keck Foundation for financial support. RMH thanks the Templeton Foundation for financial support. JS thanks the sponsors of the Indiana University Shale Research Consortium (Anadarko, Chevron, ConocoPhillips, ExxonMobil, Shell, Equinor, Marathon, Whiting, and Wintershall) for support of the IU Shale Research Lab.

Author contributions JHH and AHK conceived of the project. JHH and FH performed the simulations; JHH and AHK analyzed the results. JS and AHK collected and investigated the textural mode of apatite grains in Archean and Proterozoic shales. All authors discussed the results and wrote the manuscript.

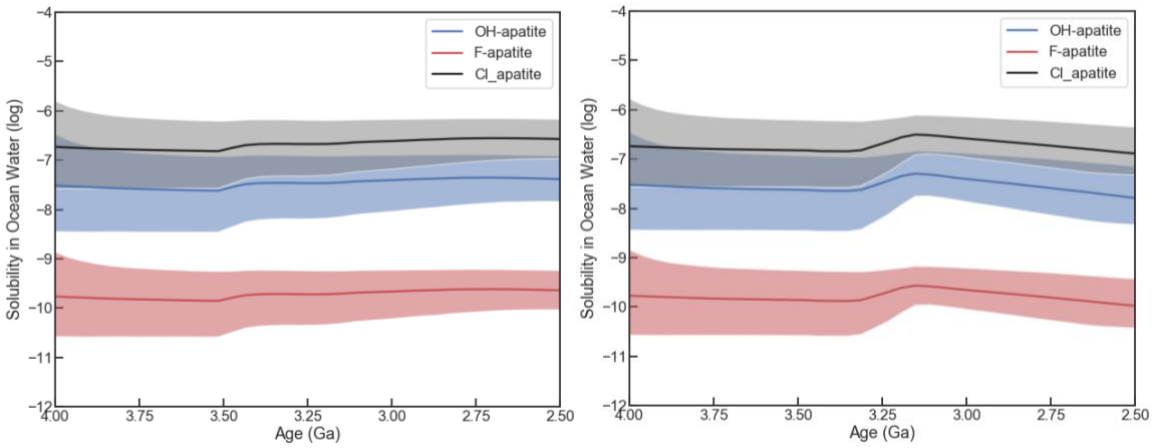

681

682 Figure 1. Limited solubilities of apatite minerals in the Archean seawater conditioned by the
683 model of a. slow continental emergence late in the Archean Eon (Flament et al., 2013); b. rapid
684 continental emergence late in the Archean Eon (Korenaga et al., 2017). Solid lines show
685 median outputs, and shaded regions show 95% confidence intervals.

686

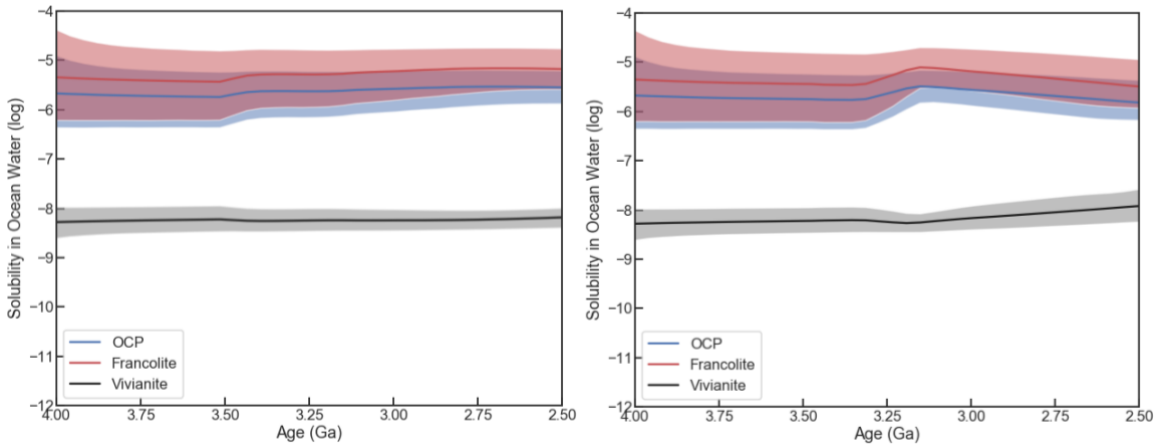

687

688 Figure 2. Solubilities of various secondary-P minerals in the Archean seawater conditioned by
689 the model of a. slow continental emergence late in the Archean Eon (Flament et al., 2013); b.
690 rapid continental emergence late in the Archean Eon (Korenaga et al., 2017). Solid lines show
691 median outputs, and shaded regions show 95% confidence intervals.

692

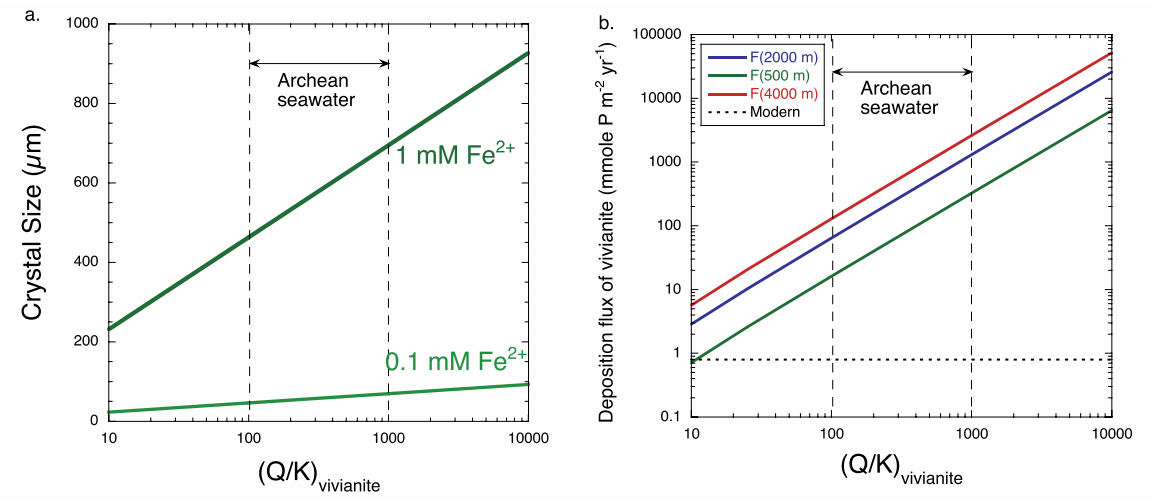

693

694 Figure 3. Precipitation of vivianite in Archean seawater: a. spiral growth (μm/yr) and b.
695 deposition flux of P as vivianite, as a log function of the probable range of supersaturation
696 states (*Q/K*) of vivianite and the thickness of the Archean ferruginous water column (colorful
697 lines in b). Dashed line in b shows the depositional flux of P in the modern ocean. Methods
698 adopted from Derry (2015).

699

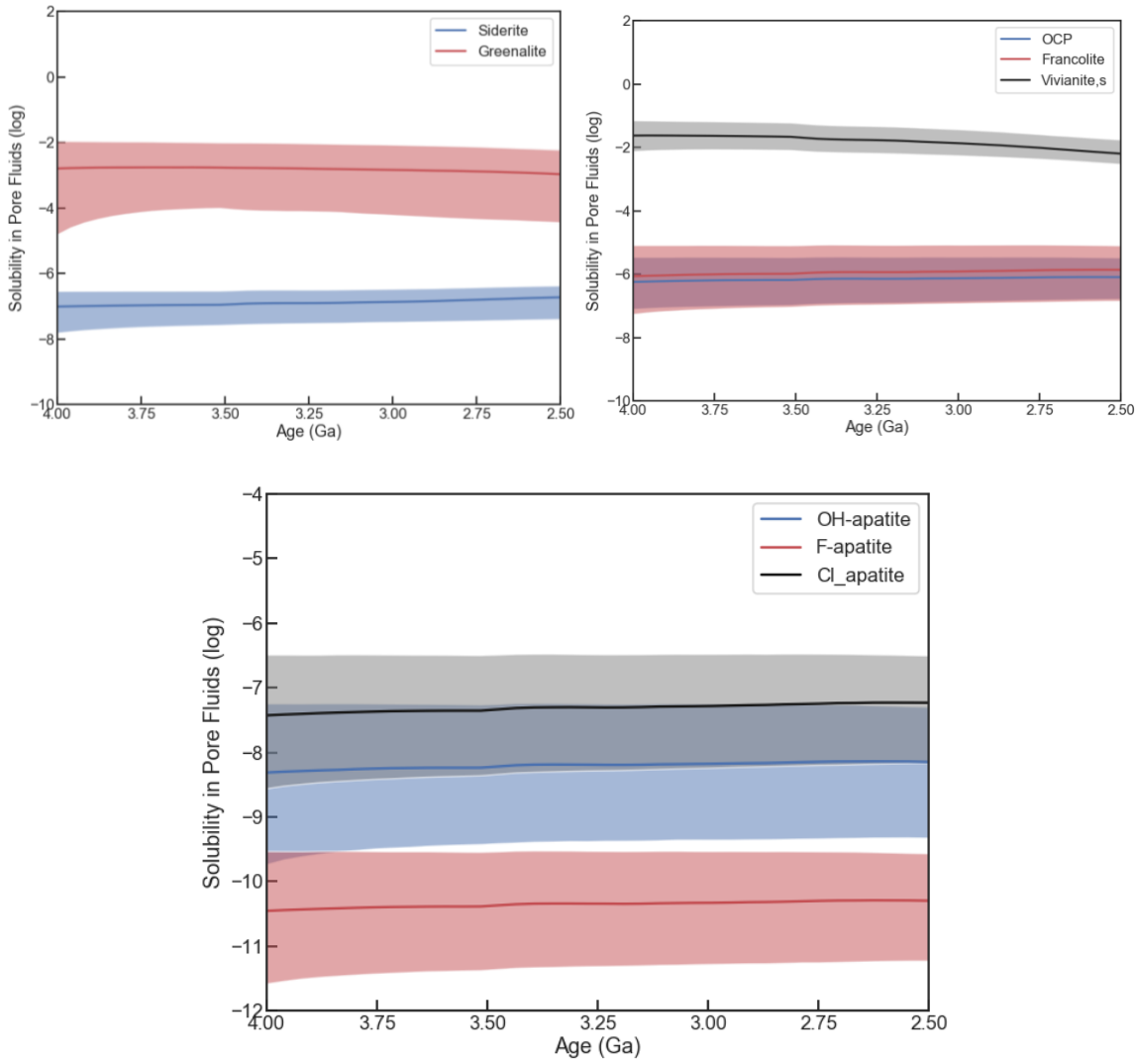

Figure 4. Solubility of siderite and greenalite (a), secondary phosphate minerals (b), and apatite minerals (c) in porewater conditioned by the model of slow continental emergence in the late Archean (Flament et al., 2013). The case of rapid continental emergence in the late Archean (Korenaga et al., 2017) is shown as supplementary Fig. S3 with similar trajectories. Solid lines show median outputs, and shaded regions show 95% confidence intervals.

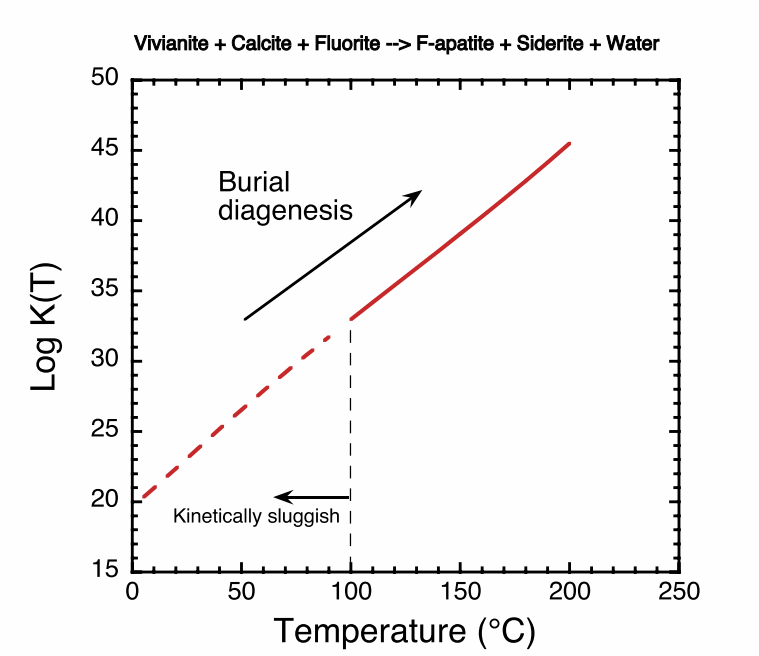

708

709 Figure 5. Transformation of vivianite into apatite during diagenesis and metamorphism:
710 equilibrium reaction constants of vivianite together with calcite and fluoride to form apatite
711 and siderite at elevated temperatures. Dashed red line indicates sluggish reaction kinetics due
712 to kinetic inhabitation of apatite and siderite precipitation at low temperatures.

713

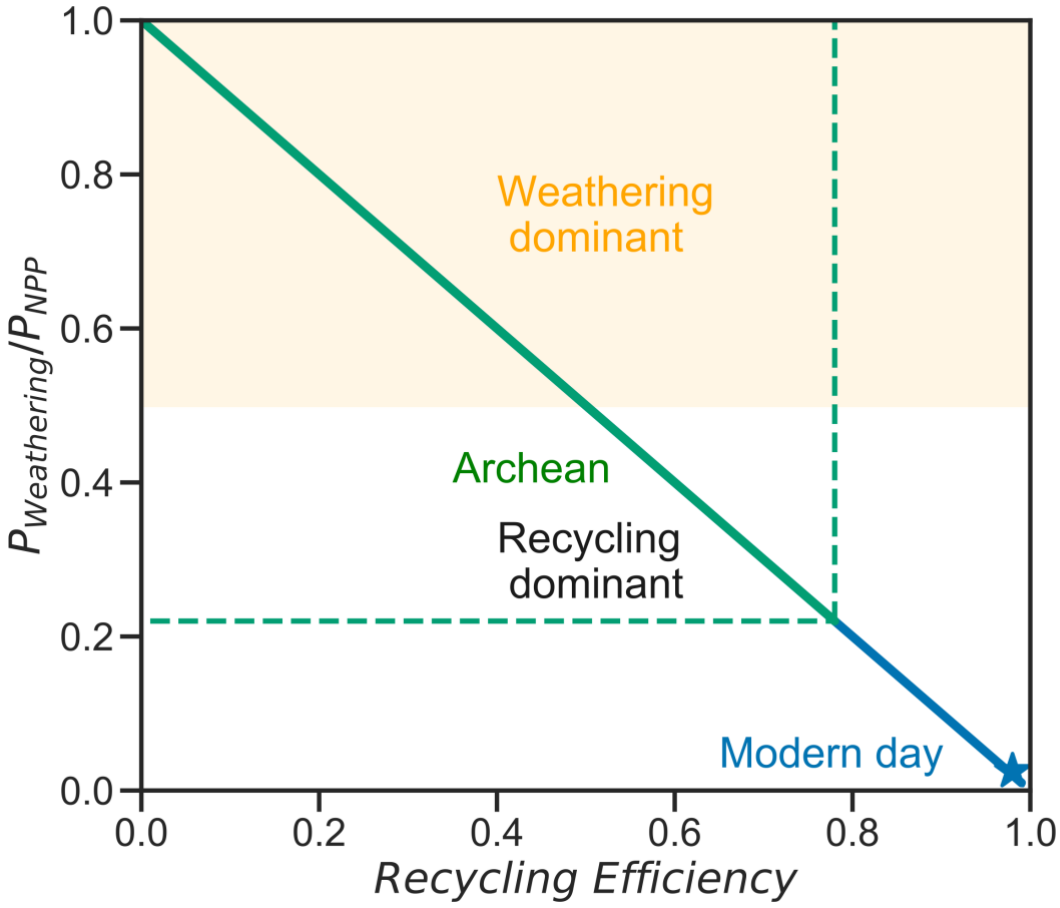

714

715 Figure 6. Proportional contribution of continental weathering flux to the total P requirement of
716 primary production plotted against recycling efficiency ($R_{recycling}$ = Recycling-P/Net primary
717 production P) of organic-P in seawater. Blue line indicates the range of modern water bodies
718 from anoxic lake ($R_{recycling}$ = in 0.78 in ferruginous Lake Matano; Crowe et al. 2011; Katsev &
719 Crowe, 2015) to oxic seawater (star; $R_{recycling}$ = 0.998). The green line shows our proposed
720 Archean case ($0.01 < R_{recycling} < 0.78$; see Sec. *4.4* for discussion), in which P recycling was
721 limited within ferruginous water.

722

723

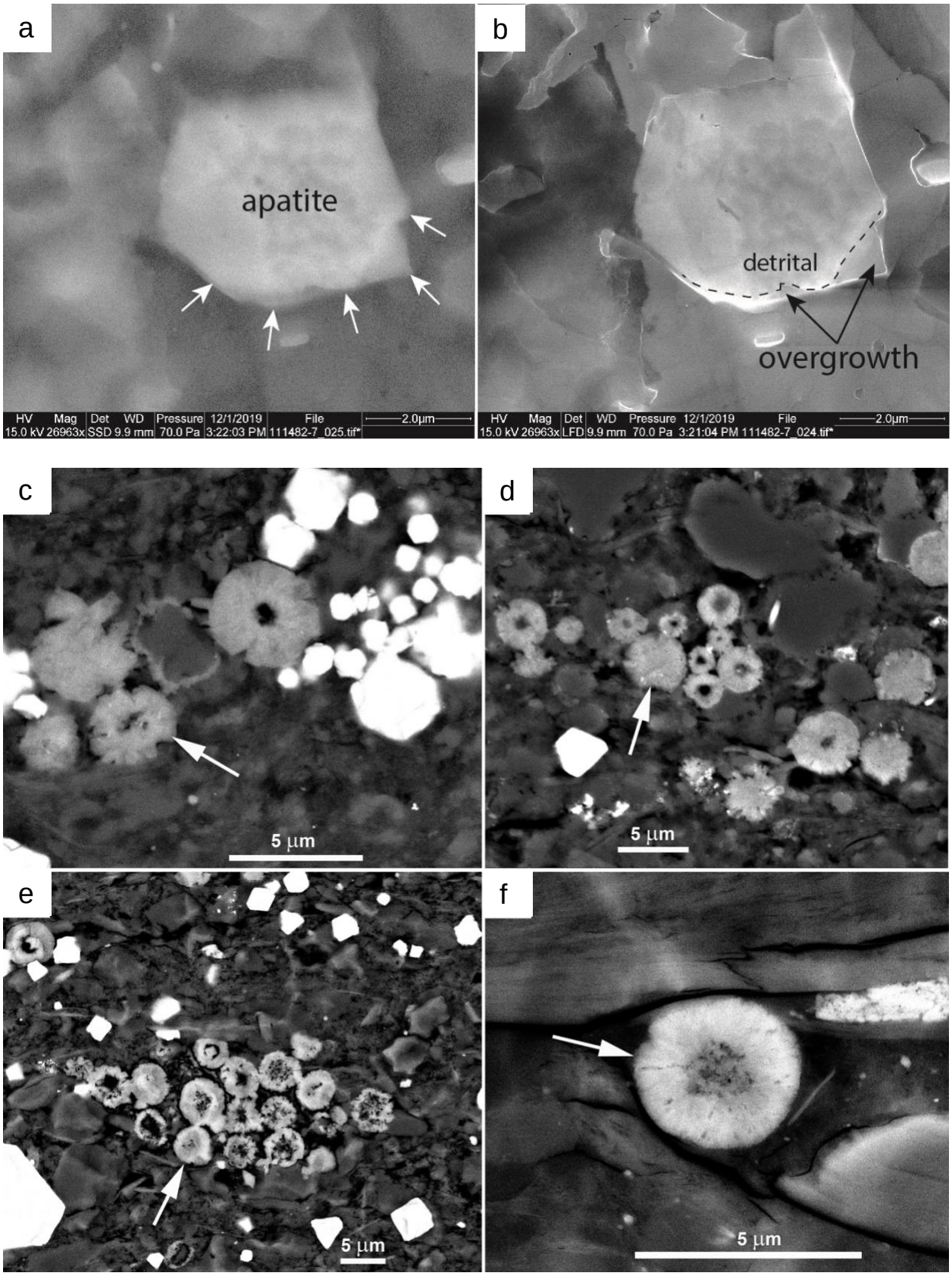

724

725 Figure 7. Contrasting appearance of apatite grains from Archean and Mesoproterozoic Archean

726 and Mesoproterozoic carbonaceous shales as imaged by scanning electron microscope (SEM).

(a) Bothaville Formation (ca. 2700 Ma), South Africa, apatite grain in center (white arrows), backscatter electron image. (b) Charge contrast in secondary electron mode allows differentiation between detrital grain and diagenetic overgrowth (dashed line) that extends into surrounding pore space. (c) Newland Formation (Belt Supergroup, Montana, USA). Note deformed thin-walled "sphere" in center of image, as well as apatite crystals projecting beyond sphere outlines. (d) Bijaigarh Shale, Vindhyan Supergroup, India, with some deformed shells and apatite crystals projecting beyond sphere outlines. (e) Velkerri Formation, Roper Group, Australia; note deformed thin-walled "spheres". (f) Solid sphere with less mineralized center portion, Kaltinsky Formation Siberia. With exception of image (b), all images were acquired with a scanning electron microscope (SEM) in backscatter mode.

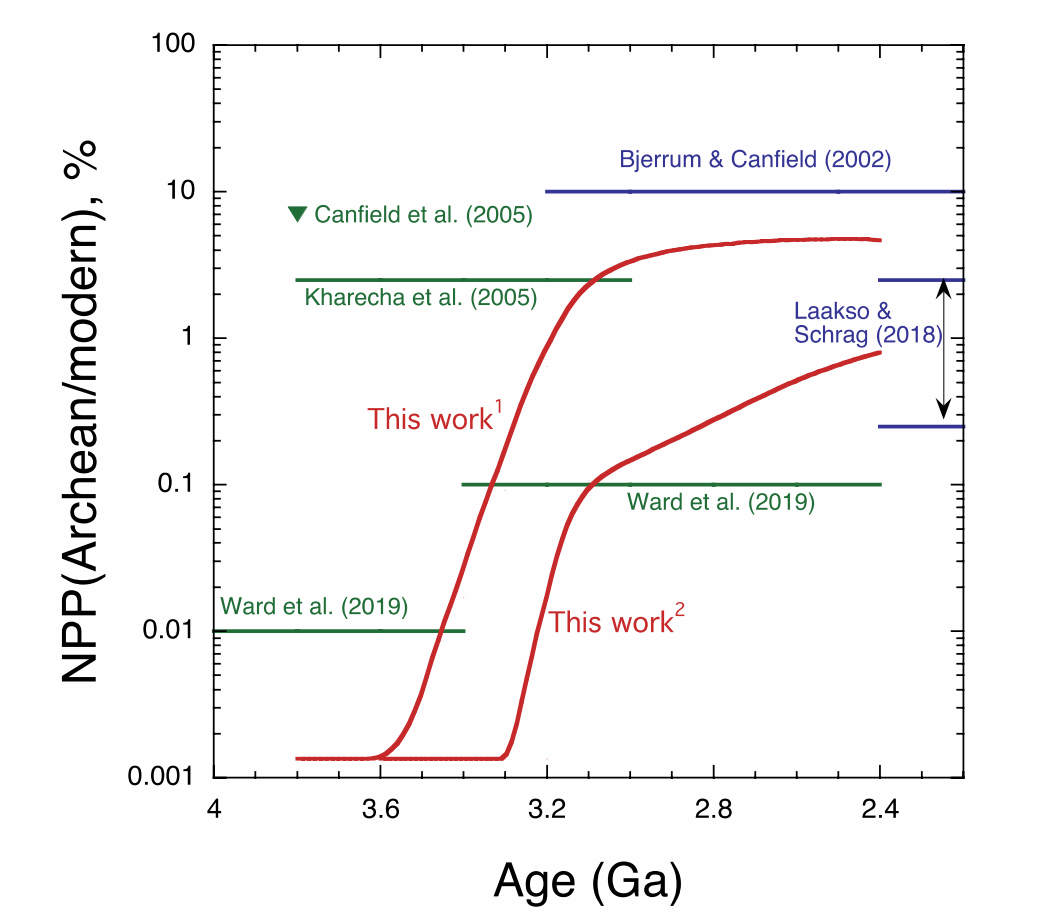

738

739 Figure 8. Upper limits of net primary production (NPP) in the ocean through the Archean Eon
740 relative to the modern level. Blue lines show the previously reported constraints (upper limit
741 or range) of NPP by the supply of P (Bjerrum & Canfield, 2002; Laakso & Schrag, 2018).
742 Green lines display the previously reported constraints (upper limits) of NPP by the supply of
743 electron donors (Canfield et al., 2005; Kharecha et al., 2005; Ward et al., 2019) and efficiency
744 of early metabolisms (Ward et al., 2019). Red curves present our reconstructed evolution
745 (upper limits) of NPP limited by the supply of P assuming: (1) slow emergence of land in the
746 late Archean (Flament et al., 2013); (2) rapid emergence of land in the late Archean (Korenaga
747 et al, 2017).

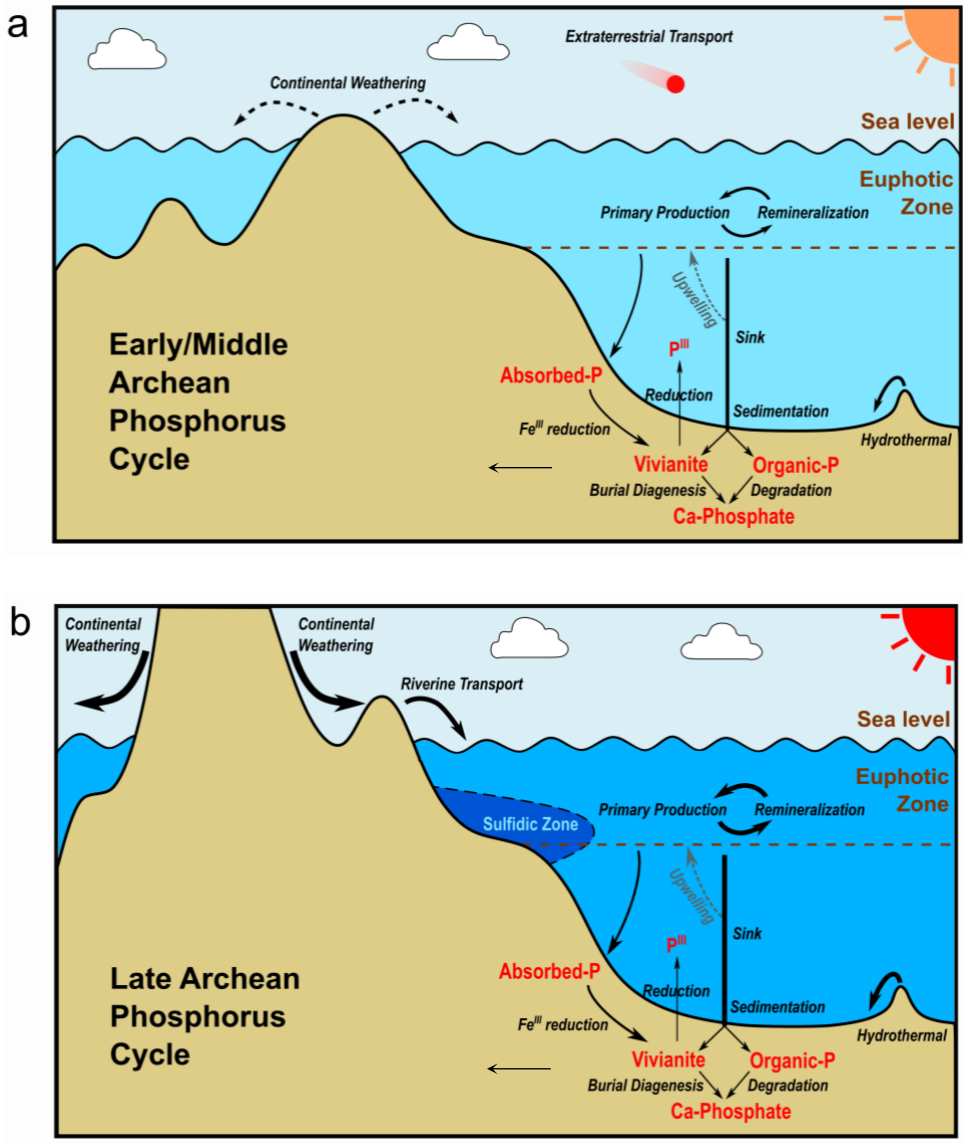

Fig. 9. Reconstructed phosphorus cycle in the early/middle Archean (a) and late Archean (b) worlds. The intensity of seawater color indicates relative levels of P, i.e. thin blue, medium blue, and dark blue represent low, medium, and high P concentration, respectively. Arrow weights indicate the relative flux of constituent processes within the P cycle (smaller flux by thin lines and greater flux by thick lines). Dashed lines or regions indicate processes presumed to be weak or only expressed locally.

758 Table 1. Fluxes of bioavailable or biological P in the modern and early Earth (in 10_{10} moles/yr).

P fluxes*	**Pre-industrial Earth**	**Early Archean Earth**	**Late Archean Earth**
Continental input[a]	10-15 [a] (+)	~0 (+)	4-34 [b] (+)
Recycling of organic P	~3710 [c] (+)	< 0.04 (+)	14-120 (+)[d]
Seafloor weathering[e]	10-36 [f] (-)	(-)	>4 (-)
Extraterrestrial	(+)	< 0.01 [g] (+)	< 0.01 (+)
Total P for net primary production[h]	3720 [c]	< 0.05	18-154

759 *Plus sign (+) represents source and minus sign (-) sink.

760 [a]Reactive P = Dissolved inorganic P + Dissolved organic P + Particulate organic P + Iron-
761 bound particulate P + Reactive aeolian P (Compton et al., 2010); [b]Hao et al. (2020); [c]Schlesiner
762 & Bernhardt (2013); [d]Optimisitic estimate calculated with equation (6-8) assuming $R_{recycling}$ =
763 0.78 (Sec. 3.3 in main text); [e]Seafloor weathering (-) = hydrothermal deposition (-) + seafloor
764 sedimentation (-) = continental input (+) + extraterrestrial input (+); [f]Paytan & McLaughlin
765 (2007); [g]Tsukamoto et al. (2018); [h]NPP(P) = continental input + recycling of organic P +
766 extraterrestrial

767

Research Data Thermodynamic properties of chemical reactions are provided in supplementary file. The continental weathering and seawater chemistry models are calculated using the codes shared online by Krissansen-Totton (https://github.com/joshuakt/early-earth-carbon-cycle) with additional modifications on continental emergence (see main text).

References:

Al-Borno A. and Tomson M. B. (1994) The temperature dependence of the solubility product constant of vivianite. *Geochim. Cosmochim. Acta* **58**, 5373–5378.

Alt, J.C. and Honnorez, J. (1984) Alteration of the upper oceanic crust, DSDP site 417: mineralogy and chemistry. *Contrib. Mineral. Petr.* 87, 149-169.

Anbar A. D., Duan Y., Lyons T. W., Arnold G. L., Kendall B., Creaser R. A., Kaufman A. J., Gordon G. W., Scott C., Garvin J. and Buick R. (2007) A whiff of oxygen before the great oxidation event? *Science (80-.).* **317**, 1903–1906.

Anderson A. T. and Greenland L. P. (1969) Phosphorus fractionation diagram as a quantitative indicator of crystallization differentiation of basaltic liquids. *Geochim. Cosmochim. Acta* **33**, 493–505.

Baturin G. (2003) Phosphorus cycle in the ocean. *Lithol. Miner. Resour.* **38**, 101–119.

Bindeman I. N., Zakharov D. O., Palandri J., Greber N. D., Dauphas N., Retallack G. J., Hofmann A., Lackey J. S. and Bekker A. (2018) Rapid emergence of subaerial landmasses and onset of a modern hydrologic cycle 2.5 billion years ago. *Nature* **557**, 545–548.

Bjerrum C. J. and Canfield D. E. (2002) Ocean productivity before about 1.9 Gyr ago limited by phosphorus adsorption onto iron oxides. *Nature* **417**, 159–162.

Borch T. and Fendorf S. (2007) Chapter 12 Phosphate Interactions with Iron (Hydr)oxides: Mineralization Pathways and Phosphorus Retention upon Bioreduction. In *Developments in Earth and Environmental Sciences* (eds. M. O. Barnett and D. B. Kent). Elsevier. pp. 321–348.

Brantley S. L. and Olsen A. A. (2014) Reaction Kinetics of Primary Rock-Forming Minerals under Ambient Conditions. In *Treatise on Geochemistry: Second Edition* (eds. H. D. Holland and K. K. Turekian). Elsevier, Oxford. pp. 69–113.

798 Brunet F. and Chazot G. (2001) Partitioning of phosphorus between olivine, clinopyroxene
799 and silicate glass in an spinel lherzolite xenolith from Yemen. *Chem. Geol.* **176**, 51–72.
800 Byrne R. H. and Kim K. H. (1993) Rare earth precipitation and coprecipitation behavior: The
801 limiting role of PO43- on dissolved rare earth concentrations in seawater. *Geochim.*
802 *Cosmochim. Acta* **57**, 519–526.
803 Canfield D. E., Rosing M. T. and Bjerrum C. (2006) Early anaerobic metabolisms. *Philos.*
804 *Trans. R. Soc. B Biol. Sci.* **361**, 1819–1834.
805 Cardona T., Sánchez-Baracaldo P., Rutherford A. W. and Larkum A. W. (2019) Early
806 Archean origin of Photosystem II. *Geobiology* **17**, 127–150.
807 Chameides W. L. and Walker J. C. G. (1981) Rates of fixation by lightning of carbon and
808 nitrogen in possible primitive atmospheres. *Orig. Life* **11**, 291–302.
809 Clark L. L., Ingall E. D. and Benner R. (1998) Marine phosphorus is selectively
810 remineralized. *Nature* **393**, 426.
811 Compton J., Mallinson D., Glenn C. R., Filippelli G., Follmi K., Shields G. and Zanin Y.
812 (2010) Variations in the Global Phosphorus Cycle. *Mar. Authigenes. From Glob. to*
813 *Microb.*, 21–33.
814 Coogan L. A., MacLeod C. J., Dick H. J. B., Edwards S. J., Kvassnes A., Natland J. H.,
815 Robinson P. T., Thompson G. and O'Hara M. J. (2001) Whole-rock geochemistry of
816 gabbros from the Southwest Indian Ridge: Constraints on geochemical fractionations
817 between the upper and lower oceanic crust and magma chamber processes at (very)
818 slow-spreading ridges. *Chem. Geol.* **178**, 1–22.
819 Cosmidis J., Benzerara K., Morin G., Busigny V., Lebeau O., Jézéquel D., Noël V., Dublet
820 G. and Othmane G. (2014) Biomineralization of iron-phosphates in the water column of
821 Lake Pavin (Massif Central, France). *Geochim. Cosmochim. Acta* **126**, 78–96.
822 Crowe S. A., Katsev S., Leslie K., Sturm A., Magen C., Nomosatryo S., Pack M. A., Kessler

J. D., Reeburgh W. S., Roberts J. A., González L., Douglas Haffner G., Mucci A., Sundby B. and Fowle D. A. (2011) The methane cycle in ferruginous Lake Matano. *Geobiology* **9**, 61–78.

de Kanel J. and Morse J. W. (1978) The chemistry of orthophosphate uptake from seawater on to calcite and aragonite. *Geochim. Cosmochim. Acta* **42**, 1335–1340.

Derry L. A. (2015) Causes and consequences of mid-Proterozoic anoxia. *Geophys. Res. Lett.* **42**, 8538–8546.

Eanes E. D. and Meyer J. L. (1977) The maturation of crystalline calcium phosphates in aqueous suspensions at physiologic pH. *Calcif. Tissue Res.* **23**, 259–269.

Falkowski P. G. (1997) Evolution of the nitrogen cycle and its influence on the biological sequestration of CO2 in the ocean. *Nature* **387**, 272–275.

Field C. B., Behrenfeld M. J., Randerson J. T. and Falkowski P. (1998) Primary production of the biosphere: Integrating terrestrial and oceanic components. *Science (80-.).* **281**, 237–240.

Fischer W. W., Hemp J. and Johnson J. E. (2016) Evolution of Oxygenic Photosynthesis. *Annu. Rev. Earth Planet. Sci.* **44**, 647–683.

Flament N., Coltice N. and Rey P. F. (2013) The evolution of the87Sr/86Sr of marine carbonates does not constrain continental growth. *Precambrian Res.* **229**, 177–188.

Fourqurean J. W., Zieman J. C. and Powell G. V. N. (1992) Phosphorus limitation of primary production in Florida Bay: Evidence from C:N:P ratios of the dominant seagrass Thalassia testudinum. *Limnol. Oceanogr.* **37**, 162–171.

Francko D. A. and Heath R. T. (1979) Functionally distinct classes of complex phosphorus compounds in lake water. *Limnol. Oceanogr.* **24**, 463–473.

Freeman J. S. and Rowell D. L. (1981) The adsorption and precipitation of phosphate onto calcite. *J. Soil Sci.* **32**, 75–84.

Friend C. R. L., Nutman A. P., Bennett V. C. and Norman M. D. (2008) Seawater-like trace element signatures (REE + Y) of Eoarchaean chemical sedimentary rocks from southern West Greenland, and their corruption during high-grade metamorphism. *Contrib. to Mineral. Petrol.* **155**, 229–246.

Geider R. J. and La Roche J. (2002) Redfield revisited: Variability of C:N:P in marine microalgae and its biochemical basis. *Eur. J. Phycol.* **37**, 1–17.

Green T. H. and Watson E. B. (1982) Crystallization of apatite in natural magmas under high pressure, hydrous conditions, with particular reference to "Orogenic" rock series. *Contrib. to Mineral. Petrol.* **79**, 96–105.

Guidry M. W. and Mackenzie F. T. (2003) Experimental study of igneous and sedimentary apatite dissolution. *Geochim. Cosmochim. Acta* **67**, 2949–2963.

Gunnars A., Blomqvist S. and Martinsson C. (2004) Inorganic formation of apatite in brackish seawater from the Baltic Sea: An experimental approach. *Mar. Chem.* **91**, 15-26.

Halevy I. and Bachan A. (2017) The geologic history of seawater pH. *Science (80-.).* **355**, 1069–1071.

Hamilton T. L. (2019) The trouble with oxygen: The ecophysiology of extant phototrophs and implications for the evolution of oxygenic photosynthesis. *Free Radic. Biol. Med.* **in press**. Doi: 10.1016/j.freeradbiomed.2019.05.003

Hansen B. C. H. and Poulsen I. F. (1999) Interaction of synthetic sulphate green rust with phosphate and the crystallization of vivianite. *Clays Clay Miner.* **47**, 312–318.

Hao J., Sverjensky D. A. and Hazen R. M. (2017) Mobility of nutrients and trace metals during weathering in the late Archean. *Earth Planet. Sci. Lett.* **471**, 148–159.

Hao J., Sverjensky D. A. and Hazen R. M. (2019) Redox states of Archean surficial environments: The importance of H2,g instead of O2,g for weathering reactions. *Chem.*

873 *Geol.* **521**, 49–58.
874 Hao J., Knoll A. H., Huang F., Hazen R. M. and Daniel I. (2020) Cycling Phosphorus on the
875 Archean Earth: Part I. Continental weathering and riverine transport of phosphorus.
876 *Geochim. Cosmochim. Acta* **273**, 70–84.
877 Hartnett H. E., Keil R. G., Hedges J. I. and Devol A. H. (1998) Influence of oxygen exposure
878 time on organic carbon preservation in continental margin sediments. *Nature* **391**, 572–
879 574.
880 Hawkesworth C. J., Cawood P. A., Dhuime B. and Kemp T. I. S. (2017) Earth's Continental
881 Lithosphere Through Time. *Annu. Rev. Earth Planet. Sci.* **45**, 169–198.
882 Hedges J. I., Hu F. S., Devol A. H., Hartnett H. E., Tsamakis E. and Keil R. G. (1999)
883 Sedimentary organic matter preservation: A test for selective degradation under oxic
884 conditions. *Am. J. Sci.* **299**, 529–555.
885 Hedges J. I. and Keil R. G. (1995) Sedimentary organic matter preservation: an assessment
886 and speculative synthesis. *Mar. Chem.* **49**, 81–115.
887 Herschy B., Chang S. J., Blake R., Lepland A., Abbott-Lyon H., Sampson J., Atlas Z., Kee T.
888 P. and Pasek M. A. (2018) Archean phosphorus liberation induced by iron redox
889 geochemistry. *Nat. Commun.* **9**.
890 Isson T. T. and Planavsky N. J. (2018) Reverse weathering as a long-term stabilizer of marine
891 pH and planetary climate. *Nature* **560**, 471–475.
892 Jiang C. Z. and Tosca N. J. (2019) Fe(II)-carbonate precipitation kinetics and the chemistry
893 of anoxic ferruginous seawater. *Earth Planet. Sci. Lett.* **506**, 231–242.
894 Jilbert T. and Slomp C. P. (2013) Iron and manganese shuttles control the formation of
895 authigenic phosphorus minerals in the euxinic basins of the Baltic Sea. *Geochim.*
896 *Cosmochim. Acta* **107**, 155–169.
897 Johnson B. R., Tostevin R., Gopon P., Wells J., Robinson S. A. and Tosca N. J. (2020)

898 Phosphorus burial in ferruginous SiO2-rich Mesoproterozoic sediments. *Geology* **48**,
899 92–96.
900 Johnson J. E., Muhling J. R., Cosmidis J., Rasmussen B. and Templeton A. S. (2018) Low-
901 Fe(III) Greenalite Was a Primary Mineral From Neoarchean Oceans. *Geophys. Res. Lett.*
902 **45**, 3182–3192.
903 Johnson J. W., Oelkers E. H. and Helgeson H. C. (1992) SUPCRT92: A software package for
904 calculating the standard molal thermodynamic properties of minerals, gases, aqueous
905 species, and reactions from 1 to 5000 bar and 0 to 1000°C. *Comput. Geosci.* **18**, 899–
906 947.
907 Jones C., Nomosatryo S., Crowe S. A., Bjerrum C. J. and Canfield D. E. (2015) Iron oxides,
908 divalent cations, silica, and the early earth phosphorus crisis. *Geology* **43**, 135–138.
909 Kakegawa T. (2003) Establishment of the phosphorous cycle in early Archean oceans.
910 *Geochim. Cosmochim. Acta Suppl.* **67**, 194.
911 Katsev S. and Crowe S. A. (2015) Organic carbon burial efficiencies in sediments: The
912 power law of mineralization revisited. *Geology* **43**, 607–610.
913 Kaufman A. J., Johnston D. T., Farquhar J., Masterson A. L., Lyons T. W., Bates S., Anbar
914 A. D., Arnold G. L., Garvin J. and Buick R. (2007) Late archean biospheric oxygenation
915 and atmospheric evolution. *Science (80-.).* **317**, 1900–1903.
916 Kharecha P., Kasting J. and Siefert J. (2005) A coupled atmosphere-ecosystem model of the
917 early Archean earth. *Geobiology* **3**, 53–76.
918 Kipp M. A. (2019) Causes and consequences of high burial efficiency in the Archean ocean.
919 In *2nd Geobiology Society Conference*
920 Kipp M. A. and Stüeken E. E. (2017) Biomass recycling and Earth's early phosphorus cycle.
921 *Sci. Adv.* **3**.
922 Konhauser K. O., Lalonde S. V, Amskold L. and Holland H. D. (2007) Was there really an

923 Archean phosphate crisis? *Science (80-.).* **315**, 1234.
924 Kopp R. E., Kirschvink J. L., Hilburn I. A. and Nash C. Z. (2005) The Paleoproterozoic
925 snowball Earth: A climate disaster triggered by the evolution of oxygenic
926 photosynthesis. *Proc. Natl. Acad. Sci.* **102**, 11131–11136.
927 Korenaga J., Planavsky N. J. and Evans D. A. D. (2017) Global water cycle and the
928 coevolution of the Earth's interior and surface environment. *Philos. Trans. R. Soc. A*
929 *Math. Phys. Eng. Sci.* **375**.
930 Kraal P., Dijkstra N., Behrends T. and Slomp C. P. (2017) Phosphorus burial in sediments of
931 the sulfidic deep Black Sea: Key roles for adsorption by calcium carbonate and apatite
932 authigenesis. *Geochim. Cosmochim. Acta* **204**, 140–158.
933 Krajewski K. P., Cappellen P. van, Trichet J., Kuhn O., LuCAs J., Martín-Algarra A., Prevot
934 L., Tewari V. C., Gaspar L. and Knight R. I. (1994) Biological processes and apatite
935 formation in sedimentary environments. *Eclogae Geol. Helv.* **87**, 701–746.
936 Krissansen-Totton J., Arney G. N. and Catling D. C. (2018) Constraining the climate and
937 ocean pH of the early Earth with a geological carbon cycle model. *Proc. Natl. Acad.*
938 *Sci.*, 201721296.
939 Kuntz L. B., Laakso T. A., Schrag D. P. and Crowe S. A. (2015) Modeling the carbon cycle
940 in Lake Matano. *Geobiology* **13**, 454–461.
941 Laakso T. A. and Schrag D. P. (2018) Limitations on Limitation. *Global Biogeochem. Cycles*
942 **32**, 486–496.
943 Lenstra W. K., Egger M., van Helmond N. A. G. M., Kritzberg E., Conley D. J. and Slomp C.
944 P. (2018) Large variations in iron input to an oligotrophic Baltic Sea estuary: impact on
945 sedimentary phosphorus burial. *Biogeosciences Discuss.* **15**, 6979–6996.
946 Lepland A., Arrhenius G. and Cornell D. (2002) Apatite in early Archean Isua supracrustal
947 rocks, southern West Greenland: Its origin, association with graphite and potential as a

948 biomarker. *Precambrian Res.* **118**, 221–241.
949 Liu J., Cheng X., Qi X., Li N., Tian J., Qiu B., Xu K. and Qu D. (2018) Recovery of
950 phosphate from aqueous solutions via vivianite crystallization: Thermodynamics and
951 influence of pH. *Chem. Eng. J.* **349**, 37–46.
952 Logan G. A., Hayes J. M., Hieshima G. B. and Summons R. E. (1995) Terminal Proterozoic
953 reorganization of biogeochemical cycles. *Nature* **376**, 53–56.
954 Lyons T. W. and Gill B. C. (2010) Ancient Sulfur Cycling and Oxygenation of the Early
955 Biosphere. *Elements* **6**, 93–99.
956 Madsen H. E. L. (2019) Influence of calcium and aluminum on crystallization of vivianite,
957 Fe3(PO4)2·8H2O. *J. Cryst. Growth* **526**, 125242.
958 Madsen H. E. L. and Hansen H. C. B. (2014) Kinetics of crystal growth of vivianite,
959 Fe3(PO4)2·8H2O, from solution at 25, 35 and 45 °C. *J. Cryst. Growth* **401**, 82–86.
960 Marty B., Avice G., Bekaert D. V. and Broadley M. W. (2018) Salinity of the Archaean
961 oceans from analysis of fluid inclusions in quartz. *Comptes Rendus - Geosci.* **350**, 154–
962 163.
963 Meurer W. P. and Natland J. H. (2001) Apatite compositions from oceanic cumulates with
964 implications for the evolution of mid-ocean ridge magmatic systems. *J. Volcanol.*
965 *Geotherm. Res.* **110**, 281–298.
966 Millero F., Huang F., Zhu X., Liu X. and Zhang J. Z. (2001) Adsorption and desorption of
967 phosphate on calcite and aragonite in seawater. *Aquat. Geochemistry* **7**, 33–56.
968 Murakami A., Sawaki Y., Ueda H., Orihashi Y., Machida S., and Komiya T. (2019) Behavior
969 of phosphorus during hydrothermal alteration of basalt under CO2-rich condition. In
970 *Japan Geoscience Union Meeting 2019*
971 Nancollas G. H. (1984) The Nucleation and Growth of Phosphate Minerals. In *Phosphate*
972 *Minerals* (eds. J. O. Nriagu and P. B. Moore). Springer Berlin Heidelberg, Berlin,

973 Heidelberg. pp. 137–154.
974 Olson S. L., Jansen M. and Abbot D. S. (2019) Oceanographic Constraints on Exoplanet Life.
975 *arXiv Prepr. arXiv1909.02928*.
976 Oxmann J. F. and Schwendenmann L. (2015) Authigenic apatite and octacalcium phosphate
977 formation due to adsorption–precipitation switching across estuarine salinity gradients.
978 *Biogeosciences* **12**, 723–738.
979 Paytan A. and McLaughlin K. (2007) The oceanic phosphorus cycle. *Chem. Rev.* **107**, 563–
980 576.
981 Planavsky N. J., Rouxel O. J., Bekker A., Lalonde S. V, Konhauser K. O., Reinhard C. T. and
982 Lyons T. W. (2010) The evolution of the marine phosphate reservoir. *Nature* **467**, 1088–
983 1090.
984 Rasmussen B. (2000) The impact of early-diagenetic aluminophosphate precipitation on the
985 oceanic phosphorus budget. *Mar. Authigenes. From Glob. to Microb.*, 89–101.
986 Rasmussen B., Muhling J. R., Suvorova A. and Krapež B. (2016) Dust to dust: Evidence for
987 the formation of "primary" hematite dust in banded iron formations via oxidation of iron
988 silicate nanoparticles. *Precambrian Res.* **284**, 49–63.
989 Reinhard C. T., Planavsky N. J., Gill B. C., Ozaki K., Robbins L. J., Lyons T. W., Fischer W.
990 W., Wang C., Cole D. B. and Konhauser K. O. (2017) Evolution of the global
991 phosphorus cycle. *Nature* **541**, 386–389.
992 Reinhard C. T., Raiswell R., Scott C., Anbar A. D. and Lyons T. W. (2009) A Late Archean
993 Sulfidic Sea Stimulated by Early Oxidative Weathering of the Continents. *Science*
994 *(80-.).* **326**, 713–716.
995 Rothe M., Kleeberg A., Grüneberg B., Friese K., Pérez-Mayo M. and Hupfer M. (2015)
996 Sedimentary sulphur:iron ratio indicates vivianite occurrence: A study from two
997 contrasting freshwater systems. *PLoS One* **10**.

998 Rothe M., Kleeberg A. and Hupfer M. (2016) The occurrence, identification and
999 environmental relevance of vivianite in waterlogged soils and aquatic sediments. *Earth-*
1000 *Science Rev.* **158**, 51–64.
1001 Rubinstein N., Fazio A. M., Scasso R. A. and Carey S. (2013) Association of phosphate with
1002 rhyolite glass in marine Neogene tuffs from Patagonia, Argentina. *Sedimentology* **60**,
1003 1007–1016.
1004 Ruttenberg K. C. (2014) The Global Phosphorus Cycle. In *Treatise on Geochemistry: Second*
1005 *Edition* (eds. H. D. Holland and K. K. Turekian). Elsevier, Oxford. pp. 499–558.
1006 Sánchez-Román M., Puente-Sánchez F., Parro V. and Amils R. (2015) Nucleation of Fe-rich
1007 phosphates and carbonates on microbial cells and exopolymeric substances. *Front.*
1008 *Microbiol.* **6**.
1009 Schieber J., Sur S. and Banerjee S. (2007) Benthic microbial mats in black shale units from
1010 the Vindhyan Supergroup, Middle Proterozoic of India: the challenges of recognizing
1011 the genuine article. *Atlas Microb. mat Featur. Preserv. within clastic rock Rec.*
1012 *Amsterdam, Elsevier*, 189–197.
1013 Schlesinger W. H. and Bernhardt E. S. (2013) *Biogeochemistry: an analysis of global*
1014 *change*., Academic press.
1015 Schneiderhan E., Zimmermann U., Gutzmer J., Mezger K. and Armstrong R. (2011)
1016 Sedimentary provenance of the neoarchean ventersdorp supergroup, Southern Africa:
1017 Shedding light on the evolution of the kaapvaal craton during the neoarchean. *J. Geol.*
1018 **119**, 575–596.
1019 Siever R. (1992) The silica cycle in the Precambrian. *Geochim. Cosmochim. Acta* **56**, 3265–
1020 3272.
1021 Sleep N. H. and Zahnle K. (2001) Carbon dioxide cycling and implications for climate on
1022 ancient Earth. *J. Geophys. Res.* **106**, 1373.

Staudigel H., Furnes H., McLoughlin N., Banerjee N. R., Connell L. B. and Templeton A. (2008) 3.5 billion years of glass bioalteration: Volcanic rocks as a basis for microbial life? *Earth-Science Rev.* **89**, 156–176.

Stüeken E. E., Catling D. C. and Buick R. (2012) Contributions to late Archaean sulphur cycling by life on land. *Nat. Geosci.* **5**, 722–725.

Syverson D. D., Reinhard C. T., Isson T. T., Holstege C., Katchinoff J., Tutolo B. M., Etschmann B., Brugger J. and Planavsky N. J. (2020) Anoxic weathering of mafic oceanic crust promotes atmospheric oxygenation. *arXiv Prepr. arXiv2002.07667*.

Thinnappan V., Merrifield C. M., Islam F. S., Polya D. A., Wincott P. and Wogelius R. A. (2008) A combined experimental study of vivianite and As (V) reactivity in the pH range 2–11. *Appl. Geochemistry* **23**, 3187–3204.

Tosca N. J., Guggenheim S. and Pufahl P. K. (2016) An authigenic origin for Precambrian greenalite: Implications for iron formation and the chemistry of ancient seawater. *Bull. Geol. Soc. Am.* **128**, 511–530.

Tosca N. J., Jiang C. Z., Rasmussen B. and Muhling J. (2019) Products of the iron cycle on the early Earth. *Free Radic. Biol. Med.* **in press**. Doi: 10.1016/j.freeradbiomed.2019.05.005

Tréguer P. J. and De La Rocha C. L. (2012) The World Ocean Silica Cycle. *Ann. Rev. Mar. Sci.* **5**, 477–501.

Tsukamoto Y., Kakegawa T., Graham U., Liu Z.-K., Ito A. and Ohmoto H. (2018) Discovery of Ni-Fe Phosphides in the 3.46 Ga-Old Apex Basalt: Implications on the Phosphate Budget of the Archean Oceans. *Goldschmidt Abstr*.

Tyrrell T. (1999) The relative influences of nitrogen and phosphorus on oceanic primary production. *Nature* **400**, 525–531.

Van Cappellen P. S. and Berner R. A. (1991) The formation of marine apatite: A kinetic

study. Yale University.

Vuillemin A., Wirth R., Kemnitz H., Schleicher A. M., Friese A., Bauer K. W., Simister R., Nomosatryo S., Ordoñez L., Ariztegui D., Henny C., Crowe S. A., Benning L. G., Kallmeyer J., Russell J. M., Bijaksana S., Vogel H. and Team the T. D. P. S. (2019) Formation of diagenetic siderite in modern ferruginous sediments. *Geology* **47**, 540–544.

Walpersdorf E., Koch C. B., Heiberg L., O'Connell D. W., Kjaergaard C. and Hansen H. C. B. (2013) Does vivianite control phosphate solubility in anoxic meadow soils? *Geoderma* **193**–**194**, 189–199.

Ward L. M., Kirschvink J. L. and Fischer W. W. (2016) Timescales of Oxygenation Following the Evolution of Oxygenic Photosynthesis. *Orig. Life Evol. Biosph.* **46**, 51–65.

Ward L. M., Rasmussen B. and Fischer W. W. (2019) Primary Productivity Was Limited by Electron Donors Prior to the Advent of Oxygenic Photosynthesis. *J. Geophys. Res. Biogeosciences* **124**, 211–226.

Wheat C. G., Feely R. A. and Mottl M. J. (1996) Phosphate removal by oceanic hydrothermal processes: An update of the phosphorus budget in the oceans. *Geochim. Cosmochim. Acta* **60**, 3593–3608.

Wong M. L., Charnay B. D., Gao P., Yung Y. L. and Russell M. J. (2017) Nitrogen Oxides in Early Earth's Atmosphere as Electron Acceptors for Life's Emergence. *Astrobiology* **17**, 975–983.

Xiong Y. (2019) Phosphorus cycling under different redox conditions. University of Leeds .

Xu N., Chen M., Zhou K., Wang Y., Yin H. and Chen Z. (2014) Retention of phosphorus on calcite and dolomite: speciation and modeling. *RSC Adv.* **4**, 35205–35214.

Zegeye A., Bonneville S., Benning L. G., Sturm A., Fowle D. A., Jones C. A., Canfield D. E.,

Ruby C., MacLean L. C., Nomosatryo S., Crowe S. A. and Poulton S. W. (2012) Green rust formation controls nutrient availability in a ferruginous water column. *Geology* **40**, 599–602.

Zonneveld K. A. F., Versteegh G. J. M., Kasten S., Eglinton T. I., Emeis K. C., Huguet C., Koch B. P., De Lange G. J., De Leeuw J. W., Middelburg J. J., Mollenhauer G., Prahl F. G., Rethemeyer J. and Wakeham S. G. (2010) Selective preservation of organic matter in marine environments; Processes and impact on the sedimentary record. *Biogeosciences* **7**, 483–511.